

Critical Behavior in Light Nuclear Systems: (I) Experimental Aspects

Y. G. Ma,^{1,2} J. B. Natowitz,¹ R. Wada,¹ K. Hagel,¹ J. Wang,¹ T. Keutgen,³ Z. Majka,⁴ M. Murray,⁵ L. Qin,¹ P. Smith,¹ R. Alfaro,⁶ J. Cibor,⁷ M. Cinausero,⁸ Y. El Masri,³ D. Fabris,⁹ E. Fioretto,⁸ A. Keksis,¹ M. Lunardon,⁹ A. Makeev,¹ N. Marie,¹⁰ E. Martin,¹ A. Martinez-Davalos,⁶ A. Menchaca-Rocha,⁶ G. Nebbia,⁹ G. Prete,⁸ V. Rizzi,⁹ A. Ruangma,¹ D. V. Shetty,¹ G. Souliotis,¹ P. Staszek,⁴ M. Veselsky,¹ G. Viesti,⁹ E. M. Winchester,¹ and S. J. Yennello¹

¹Cyclotron Institute, Texas A&M University, College Station, Texas, USA

²Shanghai Institute of Applied Physics, Chinese Academy of Sciences, Shanghai 201800, China

³UCL, Louvain-la-Neuve, Belgium

⁴Jagiellonian University, Krakow, Poland

⁵University of Kansas, Lawrence KS 66045

⁶Instituto de Fisica, UNAM, Mexico City, Mexico

⁷Institute of Nuclear Physics, Krakow, Poland

⁸INFN Laboratori Nazionali di Legnaro, Legnaro, Italy

⁹INFN and Dipartimento di Fisica, Padova, Italy

¹⁰LPC, Université de Caen, Caen, France

(Dated: December 2, 2024)

An extensive experimental survey of the features of the disassembly of a small quasi-projectile system with $A \sim 36$, produced in the reactions of 47 MeV/nucleon $^{40}\text{Ar} + ^{27}\text{Al}$, ^{48}Ti and ^{58}Ni , has been carried out. Nuclei in the excitation energy range of 1-9 MeV/u have been investigated employing a new method to reconstruct the quasi-projectile source. At an excitation energy ~ 5.6 MeV/nucleon many observables indicate the presence of maximal fluctuations in the de-excitation processes. These include the normalized second moments of the Campi plot and normalized variances of the distributions of order parameters such as the atomic number of the heaviest fragment Z_{max} and the total kinetic energy. The evolution of the correlation of the atomic number of the heaviest fragment with that of the second heaviest fragment and a bimodality test are also consistent with a transition in the same excitation energy region. The related phase separation parameter, S_p , shows a significant change of slope at the same excitation energy. In the same region a Δ -scaling analysis for of the heaviest fragments exhibits a transition to $\Delta = 1$ scaling which is predicted to characterize a disordered phase. The fragment topological structure shows that the rank sorted fragments obey Zipf's law at the point of largest fluctuations providing another indication of a liquid gas phase transition. The Fisher droplet model critical exponent $\tau \sim 2.3$ obtained from the charge distribution at the same excitation energy is close to the critical exponent of the liquid gas phase transition universality class. The caloric curve for this system shows a monotonic increase of temperature with excitation energy and no apparent plateau. The temperature at the point of maximal fluctuations is 8.3 ± 0.5 MeV. Taking this temperature as the critical temperature and employing the caloric curve information we have extracted the critical exponents β , γ and σ from the data. Their values are also consistent with the values of the universality class of the liquid gas phase transition. Taken together, this body of evidence strongly suggests a phase change in an equilibrated mesoscopic system at, or extremely close to, the critical point.

PACS numbers: 25.70.Pq, 24.60.Ky, 05.70.Jk

I. INTRODUCTION

Probing the liquid gas phase transition of finite nuclei is an important topic in nuclear physics since it should allow investigation of the nuclear equation of state and clarify the mechanism by which the nucleus disassembles when heated. This phase transition is expected to occur as the nucleus is heated to a moderate temperature so that it breaks up on a short time scale into light particles and intermediate mass fragments (IMF). Most efforts to determine the critical point for the expected liquid gas phase transition in finite nucleonic matter have focused on examinations of the temperature and excitation energy region [1, 2] where maximal fluctuations in the disassembly of highly excited nuclei are observed [3]. A variety of signatures have been employed in the identifi-

cation of this region [4, 5, 6, 7, 8] and several publications [9, 10, 11] have reported the observation of apparent critical behavior. Fisher Droplet Model analysis have been applied to extract critical parameters [12]. The derived parameters are very close to those observed for liquid-gas phase transitions in macroscopic systems [13]. Data from the EOS [14] and ISiS [15, 16] collaborations have been employed to construct a co-existence curve for nucleonic matter [12]. Interestingly, the excitation energy at which the apparent critical behavior is seen is closely correlated with the entry into the plateau region in the associated caloric curve [1]. Although implicit in the Fisher scaling analyses is the assumption that the point of maximal fluctuations is the critical point of the system [12, 17], other theoretical and experimental information suggest that the disassembly may occur well away from the criti-

cal point [1, 6, 18, 19, 20, 21]. In addition, recent lattice gas calculations indicate that the Fisher scaling may be observed at many different densities [22], raising doubts about previous critical point determinations. Further, applications of Δ -scaling analysis indicate that the observation of power-law mass distributions [23, 24], although necessary, is not sufficient to identify the true critical point of the system. We note also that while the role of the long range Coulomb interaction in determining the transition point has received considerable theoretical and experimental attention [20, 25, 26, 27, 28, 29] a number of questions remain as to the appropriate way to deal with the complications it introduces.

In this paper we report results of an extensive investigation of nuclear disassembly in nuclei of $A \sim 36$, excited to excitation energies as high as 9 MeV/nucleon. To our knowledge, this is the smallest system for which such an extensive analysis has been attempted. An earlier brief report on some aspects of this work appeared in Physical Review [30]. While investigating a smaller system takes us farther from the thermodynamic limit, several theoretical studies indicate that phase transition signals should still be observable [31, 32] in small systems. The choice of a lighter system for investigation has the advantage of reducing the Coulomb contributions.

Applying a wide range of methods we find that the maximum fluctuations in the disassembly of $A \sim 36$ occur at an excitation energy of 5.6 ± 0.5 MeV and a temperature of 8.3 ± 0.5 MeV. At this same point, the critical exponents describing the fragment distributions are found to be very close to those of the universality class of the liquid gas phase transition.

These observations do not guarantee critical behavior has been reached, however, in contrast to experimental results for heavier systems [1] we also find that the caloric curve for $A \sim 36$ does not exhibit a plateau at the point of maximum fluctuations. Taken together, the observations strongly suggest a phase change in an equilibrated mesoscopic system at, or extremely close to, the critical point.

The paper was organized as follows: in Sec. II we describe the set-up of our experiment; Section III presents a new method for reconstruction of the quasi-projectile source, QP; Section IV discusses some general features of the reconstructed QP; Section V explores the evidence for critical behavior in the disassembly of the QP. In Section VI, we discuss the caloric curve of the QP. In Section VII we use the scaling theory to derive the critical exponents of the transition. All those values are found to be consistent with the universality class of the liquid gas phase transition. Conclusions are presented in Section VIII.

II. EXPERIMENTAL SET-UP AND EVENT SELECTION

Using the TAMU NIMROD (Neutron Ion Multidetector for Reaction Oriented Dynamics) [33] and beams

TABLE I: NIMROD Charge Particle Array

Ring	Angle (deg)	No. of Segments	Solid Angle(src)
1	4.3	12	0.96
2	6.4	12	2.67
3	9.4	12	4.26
4	12.9	12	7.99
5	18.2	12	16.1
6	24.5	24	12.7
7	32.1	12	33.6
8	40.4	24	27.6
9	61.2	16	154
10	90.0	14	207.0
11	120.0	8	378.0
12	152.5	8	241.0

from the TAMU K500 super-conducting cyclotron, we have probed the properties of excited projectile-like fragments produced in the reactions of 47 MeV/nucleon ^{40}Ar + ^{27}Al , ^{48}Ti and ^{58}Ni . Earlier work on the reaction mechanisms of near symmetric collisions of nuclei in the $20 < A < 64$ mass region at energies near the Fermi energy have demonstrated the essential binary nature of such collisions, even at relatively small impact parameters [34]. As a result, they prove to be very useful in preparing highly excited light nuclei with kinematic properties which greatly simplify the detection and identification of the products of their subsequent de-excitation [35].

The charged particle detector array of NIMROD, which is set inside a neutron ball, includes 166 individual CsI detectors arranged in 12 rings in polar angles from $\sim 3^\circ$ to $\sim 170^\circ$. Eight forward rings have the same geometrical design as the INDRA detector, but have less granularity [36]. The angles, number of segments in each ring and solid angle of each CsI segment are given in Table I.

In these experiments each forward ring included two super-telescopes (composed of two Si-Si-CsI detectors) and three Si-CsI telescopes to identify intermediate mass fragments. The CsI detectors are Tl doped crystals read by photo-multiplier tubes. A pulse shape discrimination method using different responses of fast and slow components of the light output of the CsI crystals is employed to identify particles [37]. In the CsI detectors Hydrogen and Helium isotopes were clearly identified and Li fragments are also isolated from the heavier fragments. In the super-telescopes, all isotopes with atomic number $Z \leq 8$ were clearly identified and in all telescopes particles were identified in atomic number.

The NIMROD neutron ball, which surrounds the charged particle array, was used to determine the neutron multiplicities for selected events. The neutron ball consists of two hemispherical end caps and a central cylindrical section. The hemispheres are upstream and down-

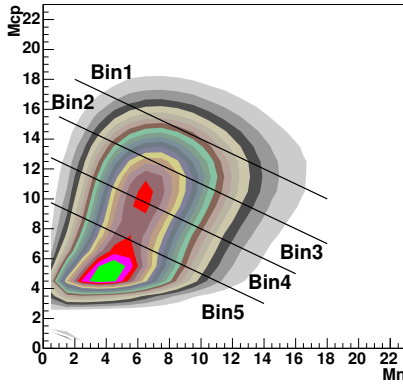


FIG. 1: (Color online) Two dimension plot for M_{cp} vs M_n as a selector of collision centrality in the $^{40}\text{Ar} + ^{58}\text{Ni}$ reaction.

stream of the charged particle array. They are 150 cm in diameter with beam pipe holes in the center. The central cylindrical sections 1.25m long with an inner hole of 60 cm diameter and 150 cm outer diameter. It is divided into four segments in the azimuthal angle direction. Between the hemispheres and the central section, there are 20 cm air gaps for cables and a duct for a pumping station. The neutron ball is filled with a pseudocumene based liquid scintillator mixed with 0.3 weight percent of Gd salt (Gd 2-ethyl hexanoate). Scintillation from a thermal neutron captured by Gd is detected by five 5-in phototubes in each hemisphere and three phototubes in each segment of the central section.

The correlation of the charged particle multiplicity (M_{cp}) and the neutron multiplicity (M_n) was used to sort event violence. In Fig. 1, lines indicate the event windows which have been explored. Roughly speaking, the more violent collisions correspond to those with the highest combined neutron multiplicity and charged particle multiplicity (M_{cp})(Bin1). This can be seen in the excitation energy distribution of the QP in Fig. 2 (the determination of excitation energy will be explained in the following section). For Bin1 and Bin2, the average excitation is ~ 4 MeV/nucleon and the E^*/A distribution extends to 9 MeV. Since the goal of the present work was to explore the disassembly of highly excited QP, we have used the data from Bin1 and Bin2 together in the present work.

Given the limitation of IMF identification in NIMROD detectors which do not have Si associated with them, the events with complete, or near complete QP detection have to be isolated before the analysis of the QP features can proceed. In the following section we describe the techniques of QP reconstruction and event selection which we have employed.

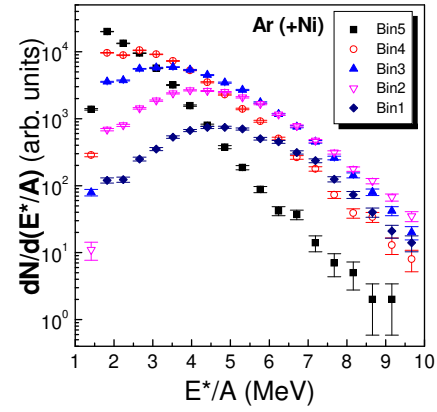


FIG. 2: (Color online) The distribution of excitation energy for different centrality bins for the QP formed in $^{40}\text{Ar} + ^{58}\text{Ni}$.

III. A NEW METHOD OF QUASI-PROJECTILE RECONSTRUCTION

Intermediate energy heavy ion collisions are complicated processes in which the roles of the mean field and nucleon-nucleon interactions may both be important. Many reactions manifest the mixed features of both the low energy deep inelastic scattering mechanism and a high energy participant-spectator mechanism.

It is well known that the laboratory frame kinetic energy spectra of most light ejectiles can be reproduced with the assumption of emission from three different sources: a Quasi- Projectile (QP) source, an intermediate velocity or Nucleon-Nucleon (NN) source and a Quasi-Target (QT) source. To better understand origins of the emitted particles the ideal situation would be to have the ability to attribute each particle to its source on an event-by-event basis. However the spectral distributions from the different sources overlap significantly, making such an attribution not possible. Previous techniques to reconstruct QP have included identifying high velocity components of the QP [38, 39] or treating only particles emitted in the forward hemisphere in the projectile frame and then assuming identical properties for particles emitted in the backward hemisphere in order to recreate the QP source [34, 40]. Such a technique is limited in its application and not suited to situations in which fluctuations are to be investigated.

For this work we have developed a new method for the assignment of each light charged particle (LCP) to an emission source. This is done with a combination of three source fits and Monte-Carlo sampling techniques. We first obtain the laboratory energy spectra for different LCP at different laboratory angles and reproduce them using the three source fits. In the laboratory frame, the energy spectra of LCP can be modelled as the overlap of emission from three independent moving equilibrated sources, *i.e.* the QP, NN and QT sources. For evaporation

from the QT source, we take [41]

$$\left(\frac{d^2N}{dE_{lab}d\Omega_{lab}}\right)_L^{QT} = \frac{M_i}{4\pi T_s^2} E'' \sqrt{E_{lab}/E'} \exp\left(-\frac{E''}{T_s}\right) \quad (1)$$

where E_{lab} and T_s are respectively the laboratory energy and apparent slope temperature. M_i are multiplicities. In the above formula, the Coulomb barrier is considered to be in the QT source frame, in this case, E' and E'' are defined as

$$E' = E_{lab} - 2\sqrt{E_{lab}\frac{1}{2}m_{LCP}v_s^2 \cos(\theta)} + \frac{1}{2}m_{LCP}v_s^2 \quad (2)$$

and

$$E'' = E' - V_C. \quad (3)$$

where v_s is the magnitude of the source velocity and is taken along the beam direction. θ is the angle between the source direction and that of the detected LCP.

For the LCP from QP and NN, we take the Coulomb barrier in the laboratory frame [42]. For QP, we assume the surface emission form

$$\left(\frac{d^2N}{dE_{lab}d\Omega_{lab}}\right)_L^{QP} = \frac{M_i}{4\pi T_s^2} \sqrt{E'E''} \exp\left(-\frac{E''}{T_s}\right). \quad (4)$$

and for NN, we take the volume emission form,

$$\left(\frac{d^2N}{dE_{lab}d\Omega_{lab}}\right)_L^{NN} = \frac{M_i}{2(\pi T_s)^{\frac{3}{2}}} \sqrt{E'} \exp\left(-\frac{E''}{T_s}\right) \quad (5)$$

where E' and E'' are defined as

$$E' = E_{lab} - V_C, \quad (6)$$

and

$$E'' = E' - 2\sqrt{E' \frac{1}{2}m_{LCP}v_s^2 \cos(\theta)} + \frac{1}{2}m_{LCP}v_s^2. \quad (7)$$

The total energy distribution is the sum over the QP, QT and NN component.

Fig. 3 shows examples of the three source fits for deuterons and tritons in the second most violent bin (*Bin2*). From these fits we know the relative contributions from the QP, NN and QT sources. Employing this information to determine the energy and angular dependent probabilities we analyze the experimental events once again and, on an event by event basis, use a Monte Carlo sampling method to assign each LCP to one of the sources QP, or NN, or QT. For example, the probability that a certain LCP i (*i.e.* p, d and t etc.) will be assigned to the QP source is

$$Prob^{QP}(E_{lab}, \theta, i) = \frac{\left(\frac{d^2N}{dE_{lab}d\Omega_{lab}}\right)_L^{QP}}{\left(\frac{d^2N}{dE_{lab}d\Omega_{lab}}\right)_L}. \quad (8)$$

To illustrate the results of such a procedure, we show, in Fig. 4, the velocity contour plots for protons to

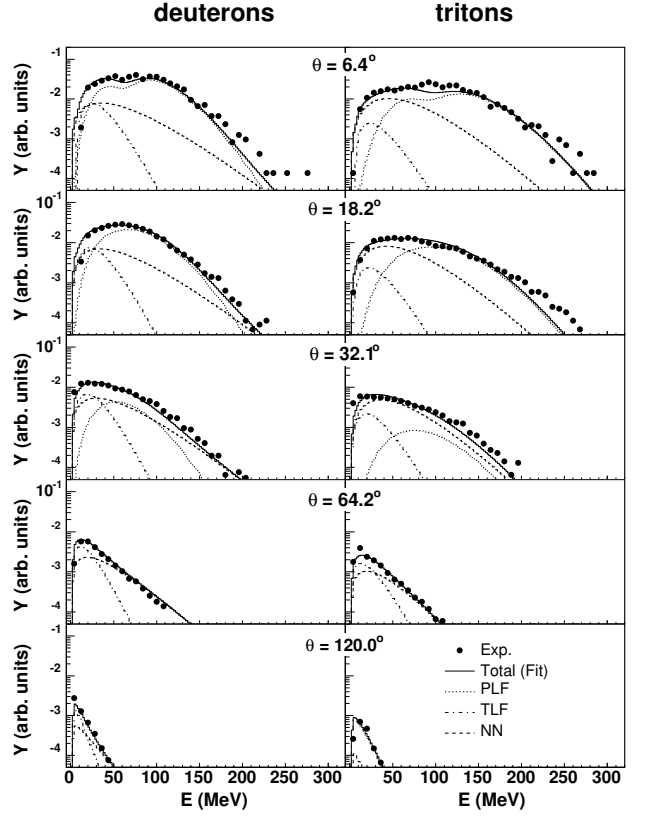


FIG. 3: The three source fits for deuterons (left panels) and tritons (right panels) in (*Bin2*) events of $^{40}\text{Ar} + ^{58}\text{Ni}$ reaction. The lab angle is $6.4^\circ, 18.2^\circ, 32.1^\circ, 64.2^\circ$ and 120° , respectively, from top to bottom. The meanings of the symbols and lines are depicted in the bottom right panel.

Lithium associated with the highest multiplicity windows in the $^{40}\text{Ar} + ^{58}\text{Ni}$ reaction.

The panels on the left represent the data before any selection, *i.e.* the raw data with contributions from all emission sources. Obviously the particles are of mixed origin and it is difficult to make a meaningful physical analysis. Since we are interested in the QP source, we show, in the middle panels, the velocity contour plots for particles assigned to the QP source using the above reconstruction method. As expected from the technique employed, the results exhibit clean, nearly spherical, velocity contours, corresponding to isotropic emission in the rest frame of QP source.

The projected parallel velocity distributions are depicted in the right panels of Fig. 4. The solid histograms represent the total distribution and the histogram with the hatched area represents the contribution from the QP source. The peak velocity of this QP contribution is close to the initial projectile velocity although some dissipation is evident.

Intermediate mass fragments, IMF, with $Z \geq 4$ were identified in the telescope modules of NIMROD. For such

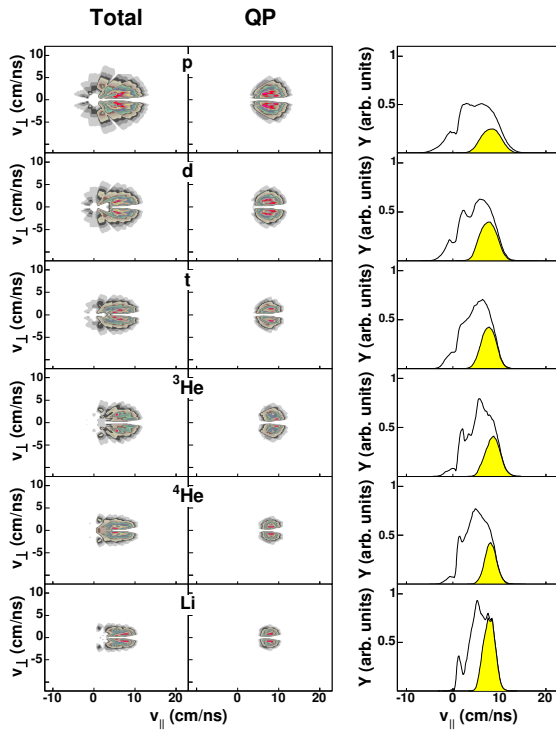


FIG. 4: (Color online) The velocity contour plots for the light charged particles in violent events (*Bin2*) of $^{40}\text{Ar} + ^{58}\text{Ni}$ reaction. From top to bottom, protons, deuterons, tritons, ^3He , ^4He and Lithium ; the left panel shows the total velocity contour plot, the middle column depicts the velocity contour plots of particles from the QP source and the right column presents the corresponding distributions of the parallel velocity from the total contribution (solid histogram) and from the QP source (hatched area). See details in text.

ejectiles we have not used such fitting techniques. Rather we have used a rapidity cut (> 0.65 beam rapidity) to assign IMF to the QP source. We also checked the sensitivity of the above rapidity cut to the results, eg., using > 0.55 and > 0.75 beam rapidity, there are only minor changes for source mass, excitation energy and temperatures etc, within $\sim 10\%$ error bars. This has no influence on any conclusions we draw in this article. Of course, this is expectable for such a binary-dominated reaction mechanism. Once we have identified all LCPs and IMFs which are assumed to come from the QP source, we can reconstruct the whole QP source on an event-by-event basis.

Fig. 5 shows the two dimensional plot of total charged particle multiplicity (M_{QP}) and total atomic number (Z_{QP}) for the reconstructed QP source. Due to the limited geometrical coverage of the telescopes, the efficiency of detection for nearly complete QP events is low. Note that the scale of z-axis of the figure is logarithmic.

To select the nearly complete QP events, we choose events with $Z_{QP} \geq 12$ (*i.e.* as good events. The parts above the line in Fig. 5) shows the good violent collisions

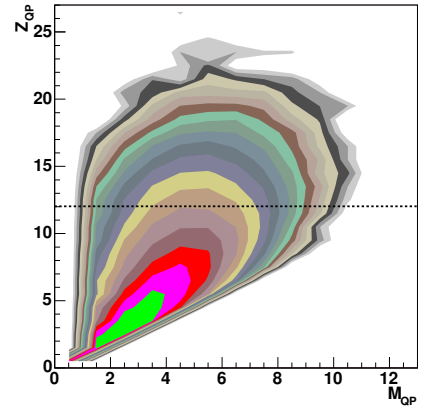


FIG. 5: (Color online) The correlation of total charge number of QP (Z_{QP}) and the total multiplicity of charged particle (M_{QP}) for the violent events of $^{40}\text{Ar} + ^{58}\text{Ni}$ reaction. The region above the dotted line is used to reconstruct the quasi-projectile. Note that the scale of z-axis is logarithmic.

for $^{40}\text{Ar} + ^{58}\text{Ni}$ reaction. The reconstructed good events in that region account for 4.3% of the total events for the violence bins selected (*Bin1* and *Bin2*). For the reactions $^{40}\text{Ar} + ^{48}\text{Ti}$ and $^{40}\text{Ar} + ^{27}\text{Al}$, the similar portion of the good central events have been collected to make the same analysis. Totally, 28000, 54000 and 56000 good QP events have been accumulated to make the following analysis for $^{40}\text{Ar} + ^{58}\text{Ni}$, ^{48}Ti and ^{27}Al reactions, respectively. For this analysis the velocity of the QP source was determined, event by event, from the momenta of all QP particles.

IV. GENERAL PROPERTIES OF THE EXCITED QP

After the reconstruction of the QP particle source, the excitation energy was deduced event-by-event using the energy balance equation [43], where the kinetic energy of charged particles (CP), the mass excesses and the (undetected) neutron contributions were considered. *i.e.*,

$$E^* = \sum_{i=1}^{M_{tot}} E_i^{kin}(CP) + \frac{3}{2} M_n T + Q \quad (9)$$

where Q , the mass excess of the QP system is determined from the mass difference between the final QP mass, A_{QP} and the sum over the masses of the detected particles of the reconstructed QP, $\sum_{i=1}^{M_{tot}} A_i(CP)$. $A_i(QP)$ is determined from the total reconstructed charge of the QP, assuming the QP has the same N/Z as the initial projectile and $A_i(CP)$ is the mass of each detected charged particle, which was calculated from the measured $Z_i(CP)$ through the numerical inversion of EPAX parameterization [44], except for $Z = 1$ and 2 for which experimental mass identification was achieved. The neutron multiplicity M_n

was obtained as the difference between the mass number (A_{QP}) of the QP and the sum of nucleons bound in the detected charged particle, i.e., $M_n = A_{QP} - \sum A_i(CP)$. $E_i^{kin}(CP)$ is the kinetic energy of the charged particles in the rest frame of QP. The contribution of the neutron kinetic energy was taken as $3/2M_n T$ with an assumed T that is equal to that of the protons. As our detector is not 100% efficient we corrected observed events (on the average) for undetected mass and energy. For a particular excitation energy bin the missing multiplicity for a given ejectile is the difference between the multiplicity derived from the source fit and the average detected ejectile multiplicity for events in the acceptance window. Assuming that missed particles have the same average kinematic properties as the detected particles of the same species allows the appropriate corrections to be made. Since almost complete projectile-like species were selected initially the missing particles were usually protons. Using these techniques we find that the average QP has a mass of 36 and a charge of 16.

Assuming the mean mass of missing particles in a given E^*/A window is equal to ΔA , the contribution of missing excitation energy ΔE^* can be approximated as $\Delta E^* = \Delta A \cdot \frac{E^*_{meas.}}{\sum A_{LCP}}$, where $E^*_{meas.}$ is the excitation energy before the correction and $\sum A_{LCP}$ is the sum of the masses of LCP ($A \leq 7$) and neutrons in the same E^*/A window. Thus the real excitation energy should be $E^*_{meas.} + \Delta E^*$. Filtering results of AMD-GEMINI calculations [45] by applying experimental acceptances leads to very similar corrections to those employed.

Fig. 6 depicts normalized excitation energy distributions for the selected QP events in $^{40}Ar + ^{27}Al$ (open circles), ^{48}Ti (open triangles) and ^{58}Ni (solid squares) for *Bin1 + Bin2*. These distributions are very similar. For violent collisions, the highest excitation energy of the QP can reach 9 MeV/nucleon. In the following analysis, we will generally separate the excitation energy distributions into 9 windows, as shown by the slices in Fig. 6. For simplicity, we sometimes identify these E^*/A windows as *Exc1* through *Exc9*.

Fig. 7 shows the total multiplicity distribution of charged particles in 9 excitation energy windows. For the quasi-projectiles formed in Ar induced reaction with different targets, the distributions keep the nearly same which is a reasonable results thanks of a clean QP reconstruction technique. Fig. 8 shows average multiplicity of LCP as a function of excitation energy. For p, d, t and 3He , the multiplicity rises monotonically but for α and Li , the multiplicities peak at E^*/A near 6 MeV/nucleon and then drop at higher excitation energy. This behavior is similar to the rise and fall behavior of IMF yield observed in many previous multifragmentation studies [46, 47, 48]. Due to the small size of our light system, this appears to occur for much smaller fragments, and even to be reflected in the $A = 4$ yields.

The QP formed in Ar + Al, Ar + Ti and Ar + Ni collisions are almost identical indicating that we have a clean technique for identifying the QP.

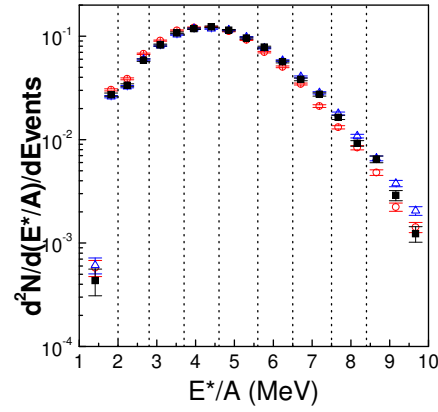


FIG. 6: (Color online) Excitation energy distribution of QP formed in $^{40}Ar + ^{27}Al$ (open circles), ^{48}Ti (open triangles) and ^{58}Ni (solid squares). Dotted lines indicate the selected excitation energy bins.

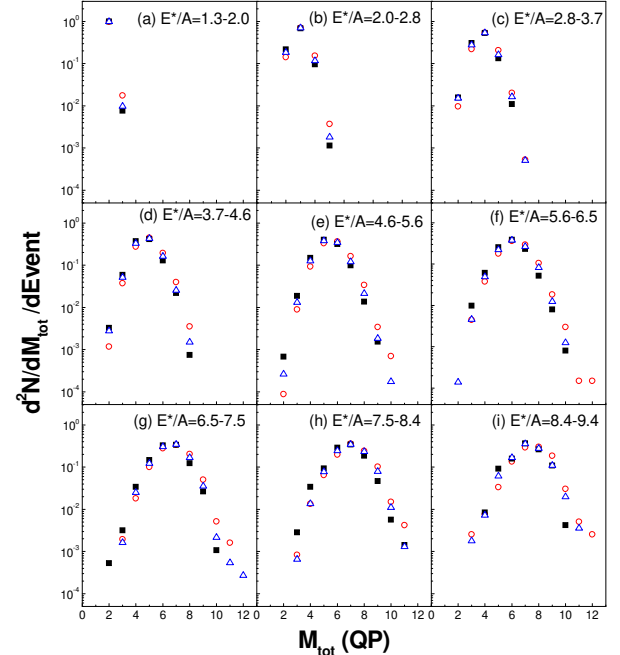


FIG. 7: (Color online) The total multiplicity distribution of charged particles from the QP systems formed in $^{40}Ar + ^{27}Al$ (open circles), ^{40}Ti (open triangles) and ^{58}Ni (solid squares).

V. EXPERIMENTAL EVIDENCE OF CRITICAL BEHAVIOR

We have used several techniques to look for evidence of possible critical behavior in the $A \sim 36$ system. These include a Fisher droplet model analysis of the charge distributions, searches for the region of maximal fluctuations using many different observables and tests of the fragment topological structure.

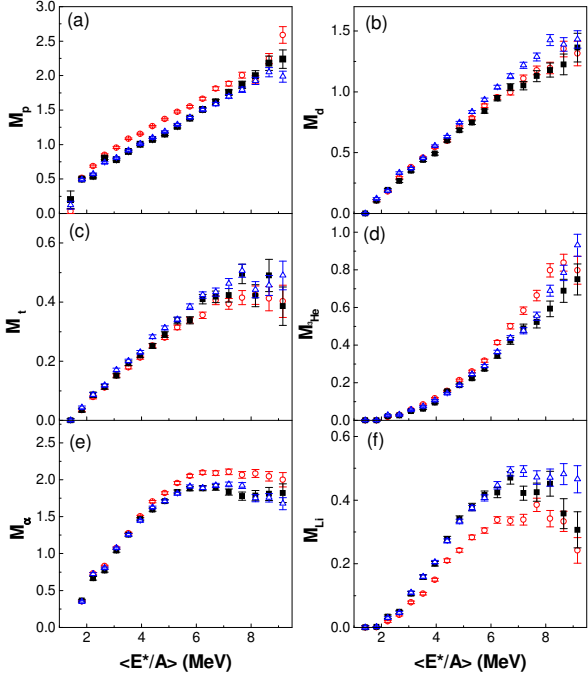


FIG. 8: (Color online) Average multiplicity of p (a), d (b), t (c), 3He (d), α (e) and Li (f) from the QP systems formed in $^{40}Ar + ^{27}Al$ (open circles), ^{40}Ti (open triangles) and ^{58}Ni (solid squares) as a function of E^*/A .

A. Fisher Droplet Model Analysis of Charge Distributions

The Fisher droplet model has been extensively applied to the analysis of multifragmentation since the pioneering experiments on high energy proton-nucleus collisions by the Purdue group [49, 50, 51]. Relative yields of fragments with $3 \leq Z \leq 14$ could be well described by a power law dependence $A^{-\tau}$ suggesting the disassembly of a system whose excitation energy was comparable to its total binding energy [50]. The extracted value of the power law exponent was $2 \leq \tau \leq 3$, which is in a reasonable range for critical behavior [13]. The success of this approach suggested that the multi-fragmentation of nuclei might be analogous to a continuous liquid to gas phase transition observed in more common fluids.

In the Fisher Droplet Model the fragment mass yield distribution, $Y(A)$, may be represented as

$$Y(A) = Y_0 A^{-\tau} X^{A^{2/3}} Y^A, \quad (10)$$

where Y_0 , τ , X and Y are parameters. However, at the critical point, $X = 1$ and $Y = 1$ and the cluster distribution is given by a pure power law

$$Y(A) = Y_0 A^{-\tau}, \quad (11)$$

The model predicts a critical exponent $\tau \sim 2.21$.

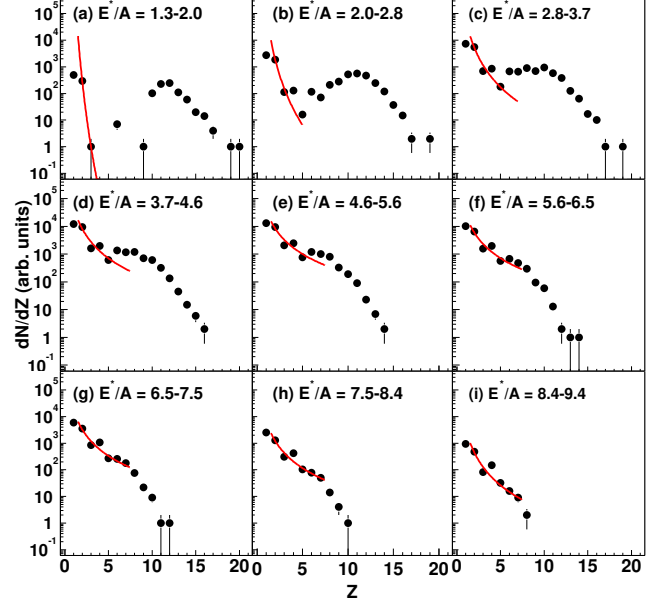


FIG. 9: (Color online) Charge distribution of QP in different E^*/A window for the reaction $^{40}Ar + ^{58}Ni$. Lines represent fits.

In Fig. 9 we present, for the QP from the reactions of $^{40}Ar + ^{58}Ni$, yield distributions, dN/dZ , observed for our nine intervals of excitation energy.

At low excitation energy a large Z residue always remains, *i.e.* the nucleus is basically in the liquid phase accompanied by some evaporated light particles. When E^*/A reaches ~ 6.0 MeV/nucleon, this residue is much less prominent. As E^*/A continues to increase, the charge distributions become steeper, which indicates that the system tends to vaporize. To quantitatively pin down the possible phase transition point, we use a power law fit to the QP charge distribution in the range of $Z = 2 - 7$ to extract the effective Fisher-law parameter τ_{eff} by

$$dN/dZ \sim Z^{-\tau_{eff}}. \quad (12)$$

The upper panel of Fig. 10 shows τ_{eff} vs excitation energy, a minimum with $\tau_{eff} \sim 2.3$ is seen to occur in the E^*/A range of 5 to 6 MeV/nucleon. $\tau_{eff} \sim 2.3$, is close to the critical exponent of the liquid gas phase transition universality class as predicted by Fisher's Droplet model [13]. The observed minimum is rather broad.

In a lattice gas model investigation of scaling and apparent critical behavior, Gulminelli *et al.* have pointed out that, in finite systems, the distribution of the maximum size cluster, *i.e.* the liquid, might overlap with the gas cluster distribution in such a manner as to mimic the critical power law behavior with $\tau_{eff} \sim 2.2$ [52]. They further note, however, that at that point the scaling laws are satisfied, which suggests a potentially more fundamental reason for the observation of the power law distribution [52]. Assuming that the heaviest cluster in each event represents the liquid phase, we have attempted to

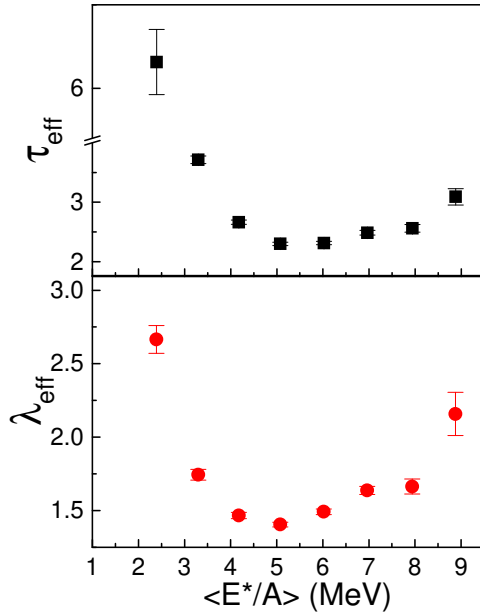


FIG. 10: (Color online) τ_{eff} and λ_{eff} as a function of excitation energy for the QP formed in $^{40}\text{Ar} + ^{58}\text{Ni}$.

isolate the gas phase by event-by-event removal of the heaviest cluster from the charge distributions. We find that the resultant distributions are better described as exponential as seen in Fig. 11.

The fitting parameter λ_{eff} of this exponential form $\exp(-\lambda_{eff}Z')$ was derived and is plotted against excitation energy in the lower panel of Fig. 10. A minimum is seen in the same region where τ_{eff} shows a minimum.

B. Maximal fluctuations

1. Campi Plots

One of the well known characteristics of the systems undergoing a continuous phase transition is the occurrence of the largest fluctuations. These large fluctuations in cluster size and density of the system arise because of the disappearance of the latent heat at the critical point. In macroscopic systems such behavior gives rise to the phenomenon of critical opalescence [53].

Campi suggested the use of event by event scatter plots of the natural log of the size of the largest cluster, $\ln A_{max}$ versus the natural log of the normalized second moment, $\ln S_2$, of the cluster distribution with the heaviest fragment removed. For our analysis we use Z_{max} as the measure of the size of the largest cluster and

$$S_2 = \frac{\sum_{Z_i \neq Z_{max}} Z_i^2 \cdot n_i(Z_i)}{\sum_{Z_i \neq Z_{max}} Z_i \cdot n_i(Z_i)}. \quad (13)$$

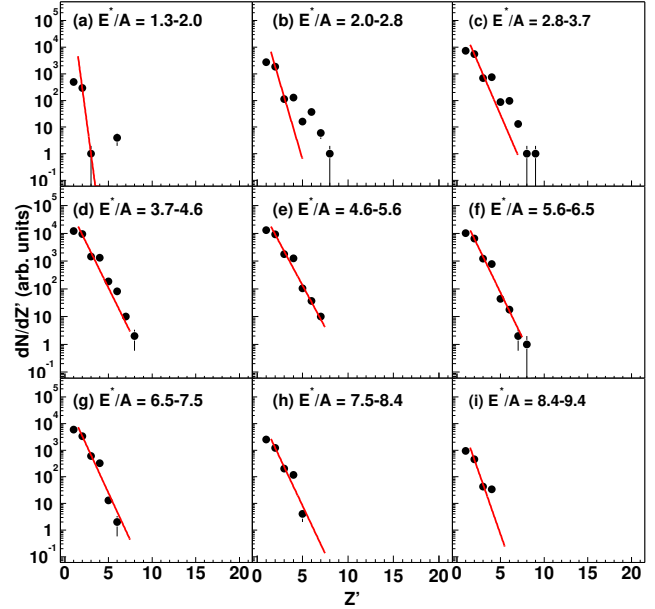


FIG. 11: (Color online) Same as Fig. 9 but the heaviest cluster is excluded on the event by event basis.

where Z_i is the charge number of QP clusters and $n_i(Z_i)$ is the multiplicity of the cluster Z_i . Campi plots have proved to be very instructive in previous searches for critical behavior [3].

In Fig. 12 we present such plots for the nine selected excitation energy bins. In the low excitation energy bins of $E^*/A \leq 3.7$ MeV/nucleon, the upper (liquid phase) branch is strongly dominant while at $E^*/A \geq 7.5$ MeV/nucleon, the lower Z_{max} (gas phase) branch is strongly dominant. In the region of intermediate E^*/A of 4.6- 6.5 MeV/nucleon, the transition from the liquid dominated branch to the vapor branch occurs, indicating that the region of maximal fluctuations is to be found in that range.

Using the general definition of the k th moment as

$$M_k = \sum_{Z_i \neq Z_{max}} Z_i^k \cdot n_i(Z_i). \quad (14)$$

Campi also suggested that the quantity, γ_2 , defined as

$$\gamma_2 = \frac{M_2 M_0}{M_1^2}, \quad (15)$$

where M_0 , M_1 and M_2 are the zeroth moment, first moment and second moment of the charge distribution, could be employed to search for the critical region. In such an analysis, the position of the maximum γ_2 value is expected to define the critical point, *i.e.*, the critical excitation energy E_c^* , at which the fluctuations in fragment sizes are the largest.

The excitation energy dependence of the average values of γ_2 obtained in an event-by-event analysis of our data

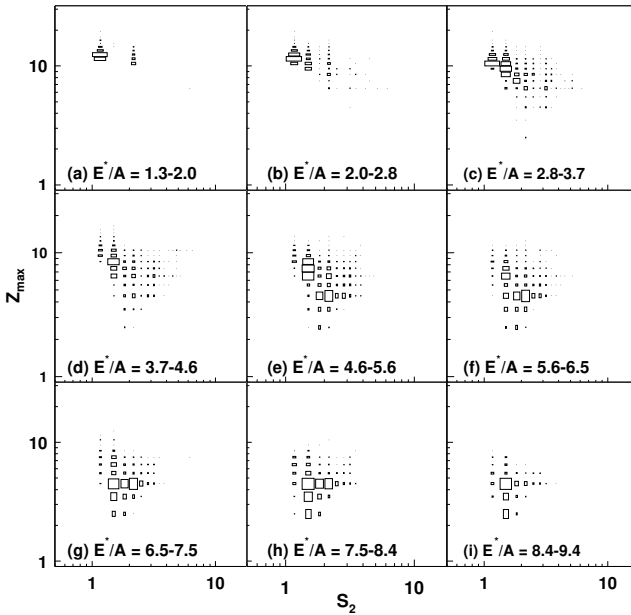


FIG. 12: (Color online) The Campi plot for different excitation energy windows for the QP formed in $^{40}\text{Ar} + ^{58}\text{Ni}$.

are shown in Fig. 13. γ_2 reaches its maximum in the 5-6 MeV excitation energy range. In contrast to observations for heavier systems [17], there is no well defined peak in γ_2 for our very light system and γ_2 is relatively constant at higher excitation energies. We note also that the peak γ_2 value is lower than 2 which is the expected smallest value for critical behavior in large systems. However, 3D percolation studies indicate that finite size effects can lead to a decrease of γ_2 with system size [54, 55]. For a percolation system with 64 sites, peaks in γ_2 under two are observed. Therefore, the lone criterion $\gamma_2 > 2$ is not sufficient to discriminate whether or not the critical point is reached. To carry out further quantitative explorations of maximal fluctuations we have investigated several other proposed observables expected to be related to fluctuations and to signal critical behavior. These are discussed below.

2. Fluctuations in the distribution of Z_{\max}

It is supposed that the cluster size distributions should manifest the maximum fluctuations around the critical point where the correlation length diverges. As a result of constraints placed by mass conservation, the size of the largest cluster should then also show large fluctuations [53]. Thus, it has been suggested that a possible signal of critical behavior is the fluctuation in the size of the maximum fragment [3]. Recently, Dorso et al. employed a molecular dynamics model to investigate fluctuations in the atomic number of the heaviest fragment (Z_{\max})

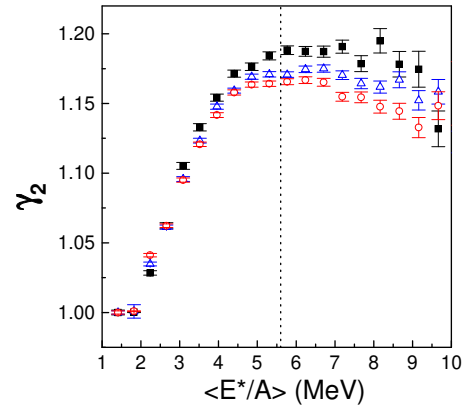


FIG. 13: (Color online) γ_2 of the QP systems formed in Ar + Al (open circles), Ti (open triangles) and Ni (solid squares) as a function of excitation energy.

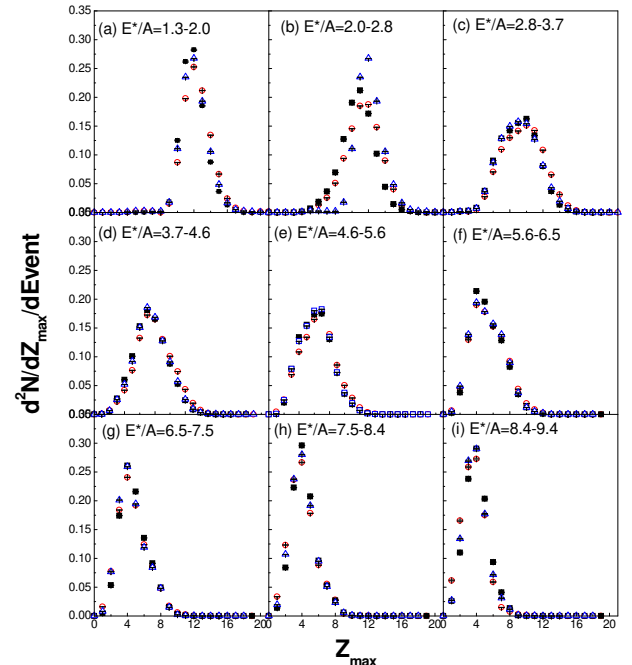


FIG. 14: (Color online) Z_{\max} distributions of the QP systems formed in Ar + Al (open circles), Ti (open triangles) and Ni (solid squares) in different excitation energy windows.

by determining its normalized variance (NVZ) [21],

$$NVZ = \frac{\sigma_{Z_{\max}}^2}{\langle Z_{\max} \rangle} \quad (16)$$

In that work, they performed calculations of the NVZ on two simple systems, one of which should not exhibit critical behavior and one which does. For the first they

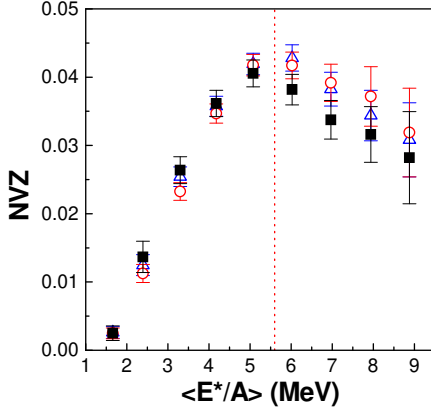


FIG. 15: (Color online) NVZ of the QP systems formed in Ar + Al (open circles), Ti (open triangles) and Ni (solid squares) as a function of excitation energy. Vertical line is at 5.6 MeV/u. See text.

used a random partition model in which the population of the different mass numbers is obtained by randomly choosing values of A following a previously prescribed mass distribution [56]. In this case the fluctuations in the populations are of statistical origin or are related to the fact that the total mass A_{tot} is fixed. No signal of criticality is to be expected. In the second case they explored the disassembly of systems of the same size employing a finite lattice bond percolation model. Such a case is known to display true critical behavior [21]. They found that that NVZ peaks close to the critical point in the percolation model calculation but shows no such peak in the random partition model calculation. This indicates that the mass conservation criterion, by itself, can not induce the peak of NVZ . The details can be found in [21].

For our data we plot the normalized variance of Z_{max} as a function of excitation energy in Fig. 15. A clear maximum, characterizing the largest fluctuation of this order parameter, is located in the $E^*/A \sim 5\text{-}6$ MeV/nucleon,

3. Fluctuations in the distribution of total kinetic energy

The system which we have studied is a hot system. If critical behavior occurs, it should also be reflected in large thermal fluctuations. Using a definition similar to that of the normalized variance of Z_{max} , we can define the normalized variance of total kinetic energy per nucleon,

$$NVE = \frac{\sigma_{E_{kin}^{tot}/A}^2}{\langle E_{kin}^{tot}/A \rangle}, \quad (17)$$

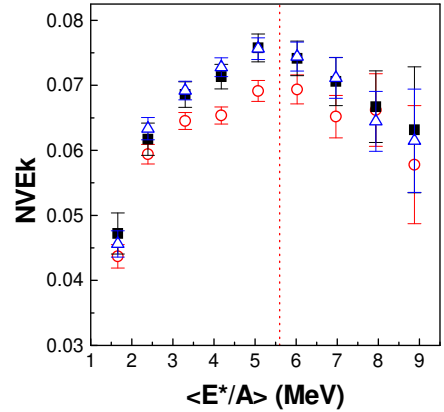


FIG. 16: (Color online) NVE of the QP systems formed in Ar + Al (open circles), Ti (open triangles) and Ni (solid squares) as a function of excitation energy. Vertical line is at 5.6 MeV/u. See text.

where E_{kin}^{tot}/A is the total kinetic energy per nucleon and $\sigma_{E_{kin}^{tot}/A}$ is its width. Fig. 16 shows the NVE as a function of excitation energy. The observed behavior is very similar to that of NVZ . Again, the maximal fluctuation was found at $E^*/A = 5\text{-}6$ MeV/u. The maximal thermal fluctuations are found in the same region as the maximal fluctuations in cluster sizes.

The use of kinetic energy fluctuations as a tool to measure microcanonical heat capacities has also been proposed [57, 58, 59].

Based on the relation of the heat capacity per nucleon and kinetic energy fluctuations, *i.e.*

$$\frac{c_V}{A_{QP}} = c \simeq c_K + c_I \simeq \frac{c_K^2}{c_K - A_{QP}\sigma_k^2/T_m^2} \quad (18)$$

where c_K and c_I are the kinetic and interaction microcanonical heat capacities per particle calculated for the most probable energy partition characterized by a microcanonical temperature T_m [57]. T_m can be estimated by inverting the kinetic equation of state [60]

$$\langle E_{kin}^{tot} \rangle = \left\langle \sum_{i=1}^M a_i \right\rangle T_m^2 + \left\langle \frac{3}{2}(M-1) \right\rangle T_m. \quad (19)$$

where $\langle \rangle$ indicates the average on the events with the same E_{kin}^{tot} and a_i is the level energy density parameter for fragment i and M is total multiplicity of QP particles. A negative heat capacity is indicated if the kinetic energy fluctuations exceed the canonical expectation $A_{QP}\sigma_k^2/T_m^2 = c_K$. In 35 MeV/nucleon Au + Au collisions, the de-excitation properties of an Au QP formed at excitation energies from 1 to 8 MeV/nucleon were investigated. Abnormal kinetic energy fluctuations were observed near the excitation energy previously identified

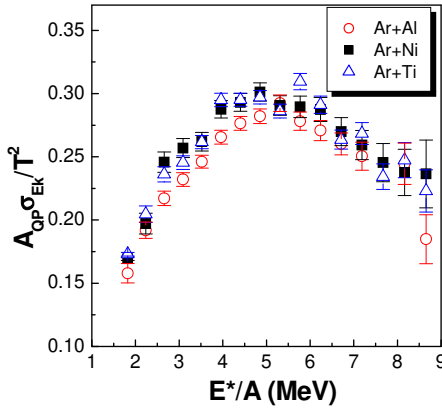


FIG. 17: (Color online) The kinetical energy fluctuation $A_{QP} \frac{\sigma_{kin}^2}{T_m^2}$ for the QP formed in $^{40}Ar + ^{27}Al$ (open circles), ^{48}Ti (open triangles) and ^{58}Ni (solid squares). See text.

as the critical energy [59] and derived negative heat capacities have been taken as a possible signal of the liquid gas phase transition.

In Fig. 17 we present the variable $A_{QP} \frac{\sigma_{kin}^2}{T_m^2}$ as a function of excitation energy as observed for the present system. The broad peak located at $E^*/A = 4.0 - 6.5$ MeV as Fig. 16 indicates the region of the largest kinetic fluctuations. We note that the value of this quantity never reaches $3/2$, which is the canonical expectation. It is possible that for such a very small system the finite size effects will limit this parameter to values well below the canonical expectation as it does for γ_2 . Hence the quantitative value of heat capacity c_V will be difficult to derive using Eq. 18 without *a priori* knowledge of c_K . It is clear that any value of c_K below 0.29 would lead to an apparent negative heat capacity.

4. Universal Scaling Laws: Δ -scaling

The recently developed theory of universal scaling laws for order-parameter fluctuations has been advanced as providing a method to select order parameters and characterize critical and non-critical behavior, without any assumption of equilibrium [61]. In this framework, universal Δ -scaling laws of the normalized probability distribution $P[m]$ of the order parameter m for different "system size" $\langle m \rangle$, should be observed:

$$\langle m \rangle^\Delta P[m] = \Phi(Z_{(\Delta)}) \equiv \Phi\left[\frac{m - m^*}{\langle m \rangle^\Delta}\right], \quad (20)$$

with $0 < \Delta \leq 1$, where $\langle m \rangle$ and m^* are the average and the most probable values of m , respectively, and $\Phi(z_{(\Delta)})$ is the (positive) defined scaling function which depends only on a single scaled variable $Z_{(\Delta)}$. If the scaling framework holds, the scaling relation is valid independent of any phenomenological reasons for changing $\langle m \rangle$ [61]. The

Δ -scaling analysis is very robust and can be studied even in small systems if the probability distributions $P[m]$ are known with a sufficient precision.

Botet *et al.* applied this universal scaling method to INDRA data for $^{136}Xe + ^{124}Sn$ collisions in the range of bombarding energies between 25 MeV/nucleon and 50 MeV/nucleon. As the relevant order parameter they chose the largest fragment charge, Z_{max} . It was found that, at $E_{lab} \geq 39$ MeV/nucleon, there is a transition in the fluctuation regime of Z_{max} . This transition is compatible with a transition from the ordered phase ($\Delta = 1/2$) to the disordered phase ($\Delta = 1$) of excited nuclear matter [23]. From this study, they attributed the fragment production scenario to the family of aggregation scenarios which includes both equilibrium models, such as the Fisher droplet model, the Ising model, or the percolation model and non-equilibrium models, such as the Smoluchowski model of gels. For such scenarios the average size of the largest cluster, $\langle Z_{max} \rangle$, is the order parameter and the cluster size distribution at the critical point obeys a power law with $\tau > 2$.

The upper panel in Fig. 18 shows that Δ -scaling of $P[Z_{max}]$ distributions for all E^*/A windows above 2.0 MeV with an assumed $\Delta = 1$. For our light system, our results show that the higher energy data are very well scaled with $\Delta = 1$ (even though not perfectly in the lower $Z_{(\Delta)}$ tail) but the lower energy data are not. Similar behaviors are also observed in other quantities, such as the total kinetic energy per nucleon E_{kin}^{tot}/A (Fig. 18(b)) and the normalized second moment S_2 (Fig. 18(c)) of QP. This indicates a transition to $\Delta = 1$ scaling in the region of $E^*/A = 5.6$ MeV. This corresponds to the fluctuations of the Z_{max} growing with the mean value, i.e. $\frac{\sigma Z_{max}}{\langle Z_{max} \rangle} \sim$ constant (see Fig. 19). The saturation of the reduced fluctuations of Z_{max} (i.e. $\frac{\sigma Z_{max}}{\langle Z_{max} \rangle}$) observed above corresponds to the transition to the regime of maximal fluctuations [24]. However the lower energy data are not well scaled by $\Delta = 1/2$.

The pattern of charged fragment multiplicity distributions $P[n]$ does not show any significant evolution with the excitation energy (Fig. 20), and the data are perfectly compressible in the scaling variables of the $\Delta = 1/2$ scaling, i.e., the multiplicity fluctuations are small in the whole excitation energy range. The scaling features of experimental Z_{max} (Fig. 18(a)) and multiplicity probability distributions (Fig. 20) are complementary and allow one to affirm that the fragment production in Fermi energy domain follows the aggregation scenario, such as the Fisher droplet model, and two phases of excited nuclear matter with distinctly different patterns of Z_{max} fluctuation. It appears that Z_{max} is a very good order parameter to explore the phase change [62].

From the studies of this section, we conclude that the largest fluctuation phase ($\Delta = 1$) is actually reached above 5.6 MeV/nucleon of excitation energy.

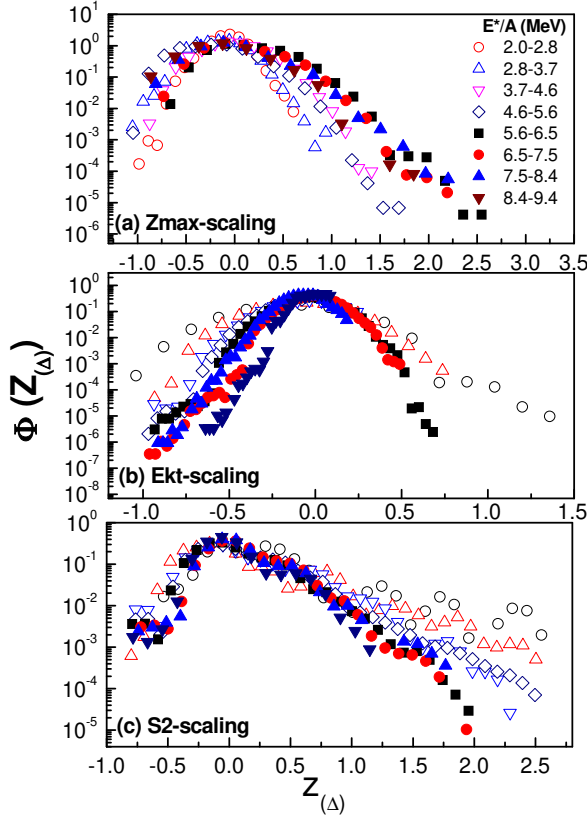


FIG. 18: (Color online) Δ -scaling for different quantities: the charge distribution of the largest fragment (a), the total kinetic energy distribution per nucleon E_{kin}^{tot}/A (b) and the normalized second moment (S_2) in different E^*/A windows. The $\Delta=1$ scaling is generally satisfied above 5.6 MeV/nucleon even it is not perfect in the lower $Z_{(\Delta)}$ tail.

C. Fragment Topological Structure

In addition to the thermodynamic and fluctuation features of the system, observables revealing some particular topological structure may also reflect the critical behavior for a finite system. For example, if we make a plot for the average value of Z_{2max} vs Z_{max} in the different excitation energy windows, we immediately see that a transition occurs near 5.6 MeV/nucleon (Fig. 21). Below that point $\langle Z_{2max} \rangle$ increases with decreasing $\langle Z_{max} \rangle$. In these energy zones, the fragmentation is basically dominated by evaporation and sequential decay is important. But above 5.6 MeV/nucleon excitation energy, $\langle Z_{2max} \rangle$ decreases with decreasing $\langle Z_{max} \rangle$. In this region of excitation, the nucleus is essentially fully vaporized and each cluster shows a similar behavior.

Below we present an exploration of two more detailed observables characterizing the topological structure, i.e., Zipf law relationships and bimodality.

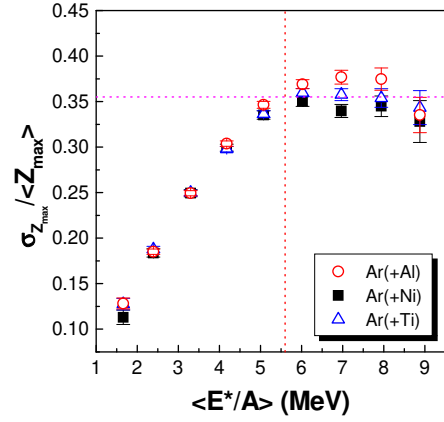


FIG. 19: (Color online) $\sigma_{Z_{max}}/\langle Z_{max} \rangle$ as a function $\langle E^*/A \rangle$ for the QP formed in $^{40}\text{Ar} + \text{Al}$ (open circles), Ni (filled squares) and Ti (open triangles).

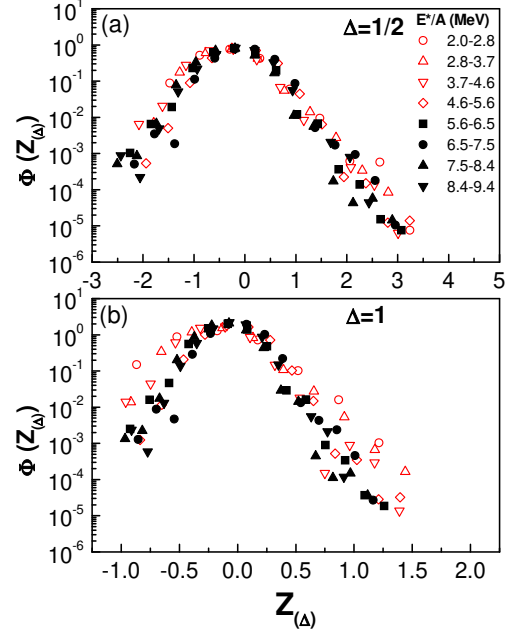


FIG. 20: (Color online) $\Delta = 1/2$ scaling of charged fragment multiplicity distributions in different E^*/A windows for the QP formed in $^{40}\text{Ar} + ^{58}\text{Ni}$.

1. Zipf plots and Zipf's law

Recently, Ma proposed measurements of the fragment hierarchy distribution as a means to search for the liquid gas phase transition a finite system [63, 64]. The fragment hierarchy distribution can be defined by the so-called Zipf plot, i.e., a plot of the relationship between mean sizes of fragments which are rank-ordered in size, i.e., largest, second largest, etc. and their rank [63, 64]. Originally the Zipf plot was used to analyze the hierarchy of usage of words in a language [65], i.e. the relative

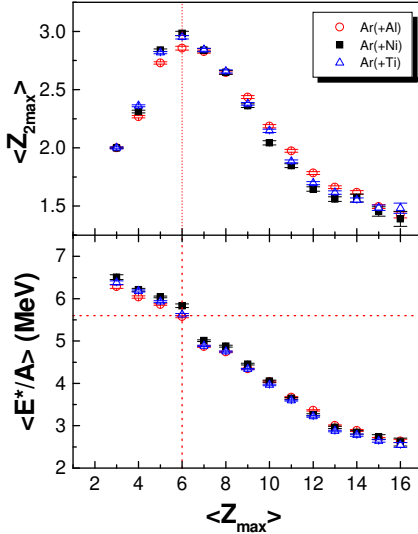


FIG. 21: (Color online) The $\langle Z_{2max} \rangle$ as a function of $\langle Z_{max} \rangle$. The mean excitation energy is shown beside of points.

population of words ranging from the word used most frequently to the word used least frequently. The integer rank was defined starting from 1 for the most probable word and continuing to the least probable word. Surprisingly, a linear relationship between the frequency and the order of words was found. Later, many more applications of this relationship were made in a broad variety of areas, such as population distributions, sand-pile avalanches, the size distribution of cities, the distribution in strengths of earthquakes, the genetic sequence and the market distribution of sizes of firms, etc. It has been suggested that the existence of very similar linear hierarchy distributions in these very different fields indicates that Zipf's law is a reflection of self-organized criticality [66].

The significance of the 5-6 MeV region in our data is further indicated by a Zipf's law analysis such as that proposed in [63, 64]. In such an analysis, the cluster size is employed as the variable to make a Zipf-type plot, and the resultant distributions are fitted with a power law ,

$$\langle Z_{rank} \rangle \propto rank^{-\xi}, \quad (21)$$

where ξ is the Zipf's law parameter. In Fig. 22 we present Zipf plots for rank ordered average Z in the nine different energy bins. Lines in the figure are fits to the power law expression of Eq.(21). Fig. 23 shows the fitted ξ parameter as a function of excitation energy. As shown in Fig. 22, this rank ordering of the probability observation of fragments of a given atomic number, from largest to the smallest, does indeed lead to a Zipf's power law parameter $\xi = 1$ in the 5-6 MeV/nucleon range. When $\xi \sim 1$, Zipf's law is satisfied. In this case, the mean size of the second largest fragment is 1/2 of that of the the largest fragment; That of the third largest fragment is 1/3 of the largest fragment, etc.

We note that the nuclear Zipf-type plot which was proposed in Ref. [63, 64] has been applied in the analysis of

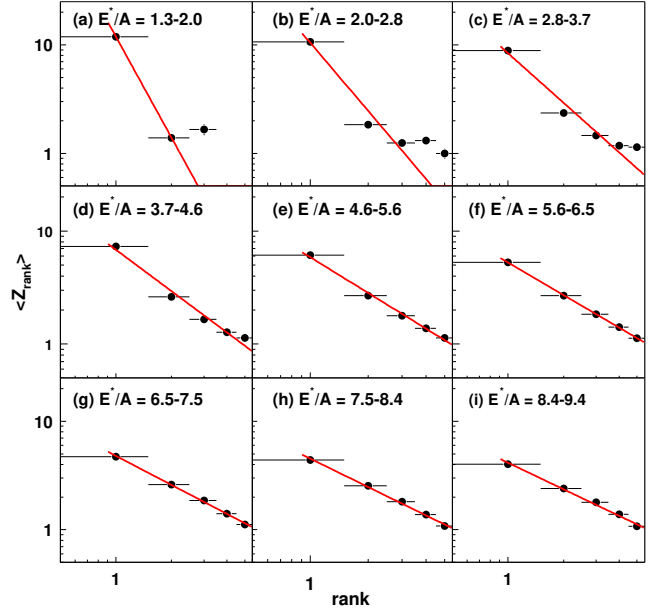


FIG. 22: (Color online) Zipf plots in nine different excitation energy bins for the QP formed in $^{40}\text{Ar} + ^{58}\text{Ni}$. The dots are data and the lines are power-law fits (Eq. 21).

CERN emulsion or Plastic data of $\text{Pb} + \text{Pb}$ or Plastic at 158 GeV/nucleon and it was found that the nuclear Zipf law is satisfied when the liquid gas phase transition occurs [67].

In a related observation which is consistent with the formulation of Zipf's law, percolation model calculations [68] suggest that the ratio $S_p = \frac{\langle Z_{2max} \rangle}{\langle Z_{max} \rangle}$ reaches 0.5 around the phase separation point. Here Z_{2max} is the atomic number of the second heaviest fragment in each event. Fig. 24 shows S_p versus E^*/A . $S_p = 0.5$ at 5.2 MeV/nucleon. It exhibits essentially linear behavior (with two different slopes) above and below that point.

2. Bimodality

Another proposed test of phase separation is bimodality which was suggested in [69]. As has been noted [70] this approach generalizes definitions based on curvature anomalies of any thermodynamic potential as a function of an observable which can then be seen as an order parameter. It interprets a bimodality of the event distribution as coexistence, each component representing a different phase. It provides a definition of an order parameter as the best variable to separate the two maxima of the distribution. In this framework when a nuclear system is in the coexistence region, the probability distribution of the order parameter is bimodal.

In analysis of INDRA data [70], $(\frac{\sum_{z_i \geq 13} Z_i - \sum_{3 \geq z_i \leq 12} Z_i}{\sum_{z_i \geq 3} Z_i})$ was chosen as a sorting parameter. This parameter may be connected with the

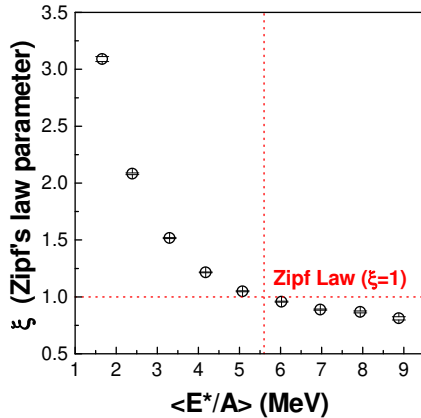


FIG. 23: (Color online) Zipf parameter as a function of excitation energy for the QP formed in $^{40}\text{Ar} + ^{58}\text{Ni}$. The position of cross illustrates the Zipf law is reached around 5.6 MeV/u excitation energy.

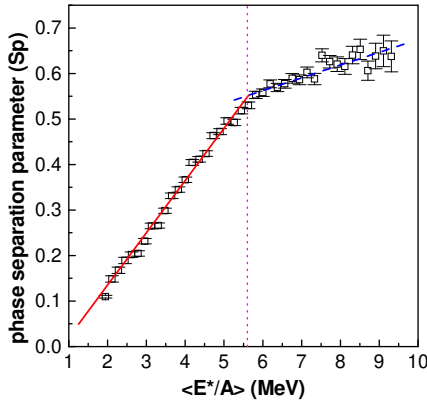


FIG. 24: (Color online) The phase separation parameter as a function of excitation energy for the QP formed in $^{40}\text{Ar} + ^{58}\text{Ni}$.

density difference of the two phases ($\rho_l - \rho_g$), which is the order parameter for the liquid gas phase transition.

For our very light system, if we consider the clusters with $Z \leq 3$ as a gas and the clusters with $Z \geq 4$ as a liquid, a parameter characterizing the bimodal nature of the distribution can be defined as

$$P = \frac{\sum_{Z_i \geq 4} Z_i - \sum_{Z_i \leq 3} Z_i}{\sum_{Z_i \geq 1} Z_i}. \quad (22)$$

Fig. 25 shows the mean value of P as a function of E^*/A .

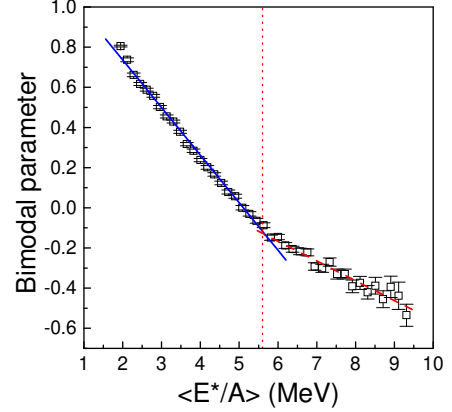


FIG. 25: (Color online) The average value of bimodal as a function of excitation energy for the QP formed in $^{40}\text{Ar} + ^{58}\text{Ni}$.

Here again, the slope shows a distinct change at $E^*/A = 5-6$ MeV where $P = 0$, *i.e.* the point of equal distribution of Z in the two phases.

VI. CALORIC CURVE

It is also interesting to ask how the caloric curve for this light system behaves. Several different experimental methods have been applied to the determination of caloric curves for nuclear systems. The most common of these are the use of slope parameters of the kinetic energy spectra or the use of isotopic yield ratios [71]. Since sequential decays and side feeding may be important in either case, corrections for such effects must normally be applied to observed or "apparent" temperatures in order to obtain the initial temperatures corresponding to the initial excitation energies of the nuclei under investigation [75, 76]. For heavier systems, a number of measurements of caloric curves have been reported [1] and references therein. In those measurements a flattening or plateauing is generally observed at higher excitation energies. For light systems such as the $A \sim 36$ system studied here there are relatively few measurements of caloric curves. For construction of the caloric curve from the present data we have used both the slope measurement and isotope ratio technique to derive "initial temperatures" from the observed apparent temperatures, limiting the use of each to its own range of applicability as discussed below.

A. Low Excitation - the Liquid-Dominated Region

Determinations based on spectral slope parameters began with fitting the kinetic energy spectra for different LCPs associated with the nine different bins in excitation energy to obtain the apparent slope temperatures T_s in the QP source frame. T_s can be obtained assuming a surface emission type Maxwellian distribution, *i.e.*,

$$\frac{d^2N}{dE_{kin}^{QP} \cdot dEvent} = c_0 \frac{E_{kin}^{QP} - V_{coul}}{T_s^2} \exp\left(-\frac{E_{kin}^{QP} - V_{coul}}{T_s}\right). \quad (23)$$

where E_{kin}^{QP} is the kinetic energy in the QP frame and V_{coul} is the barrier parameter. For an example, Fig. 26 shows the fits to the kinetic spectra of deuterons and tritons in the QP frame in four different E^*/A windows. The dashed lines represent the fits and they show excellent agreement with the data. Using such fitted results, the excitation function of T_s can be obtained for each light charged particle as shown in Fig. 27. In this figure, we also plot (dotted line) $T_s = \sqrt{8E^*/A}$ which corresponds to the temperature from a simple Fermi gas assumption. For these different particles, the apparent temperatures are different from each other since the effects of sequential decay are different for different particles. We note that the temperatures, T_s , of 3He and Li , are larger than those of other LCPs, indicating that they might be the least affected by the sequential decay effects, while T_s for *protons* shows dramatically smaller values than the others indicating that the *p* spectra are strongly influenced by later stage emissions. We then employed the measured excitation energy dependence of the multiplicity for the ejectile under consideration to derive initial temperatures from the apparent slope temperatures [72, 73].

For each LCP, the measured multiplicity is the sum over the entire de-excitation cascade. Since the temperature of an evaporation residue in an excitation energy bin characterized by a small change of excitation from E_1^* to E_2^* is, to a good approximation,

$$\langle T_{ini} \rangle = \frac{\langle M_2 \rangle \langle T_2 \rangle - \langle M_1 \rangle \langle T_1 \rangle}{\langle M_2 \rangle - \langle M_1 \rangle} \quad (24)$$

where M_2 and M_1 are the multiplicities of a certain LCP at the excitation energy E_2^* and E_1^* where $E_1^* > E_2^*$. The details of this method can be found in references [72, 73].

With this method, we can derive the initial temperatures for each particle. For each particle except protons we obtained a reasonable agreement of the respective initial temperatures and therefore use their average values, as shown by solid squares in Fig. 28, as a mean initial temperature for plotting the caloric curve. For protons, the apparent temperature is very low from fits as shown in Fig. 27 since a large portion of protons may originate from the side feeding besides the sequential decay chain. However, the former can not be corrected with Eq. (24).

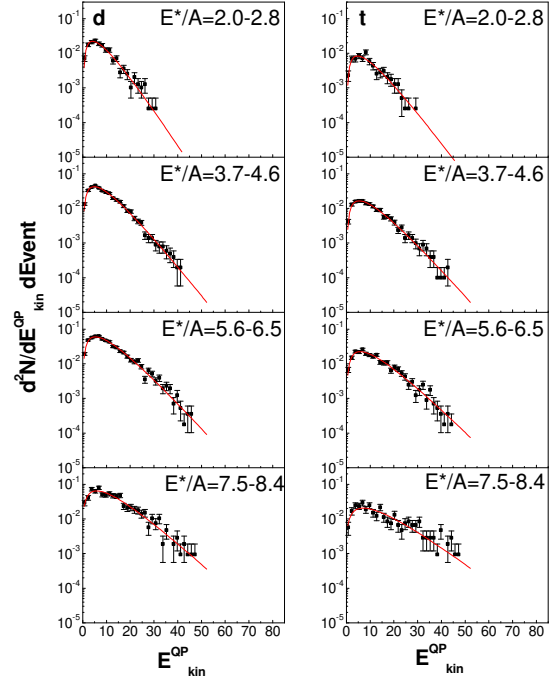


FIG. 26: (Color online) Kinetic energy spectra in the QP frame of $^{40}\text{Ar} + ^{58}\text{Ni}$ in four selected E^*/A windows. Left panels are for deuterons and right for tritons. The dots are experimental data and the lines are fits with Eq. 23.

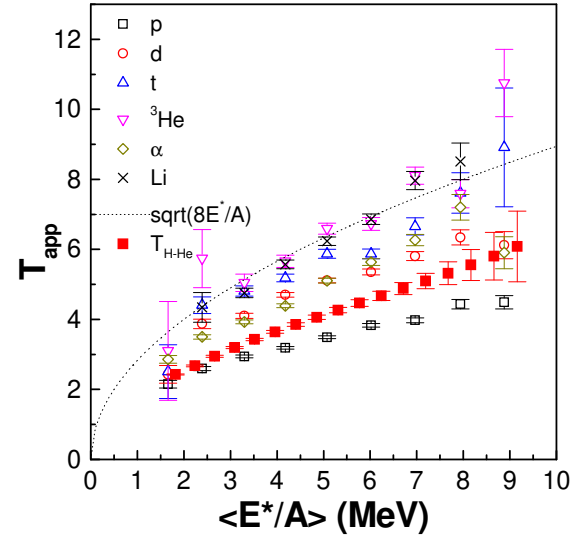


FIG. 27: (Color online) The apparent temperatures from the slopes of different particles (open symbols) and from isotopic ratio (solid squares) as a function of excitation energy for the QP formed in $^{40}\text{Ar} + ^{58}\text{Ni}$. The line is the Fermi gas model calculation: $T_s = \sqrt{8E^*/A}$.

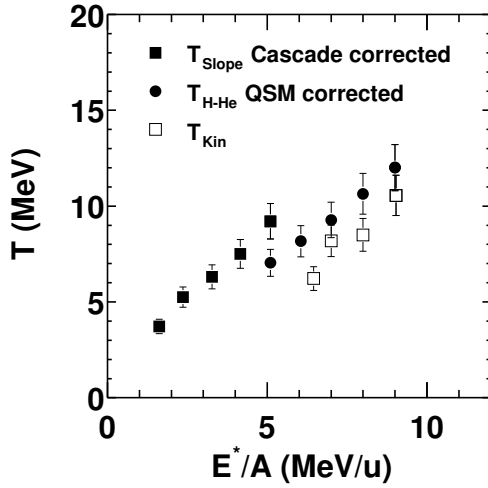


FIG. 28: (Color online) The deduced caloric curves for the QP formed in $^{40}\text{Ar} + ^{58}\text{Ni}$. The symbols are displayed in insert. See details in text.

It must be emphasized that this technique is based on the assumption of sequential evaporation of the ejectiles from a cooling compound nucleus source [72, 73]. Given that the various observables discussed above suggest an important transition at 5.6 MeV/u excitation energy, this method should not be appropriate above that energy. In fact, initial temperatures deduced using this approach exhibit a very rapid increase at excitation energies above 6 MeV/nucleon (not shown). We take this as evidence that sequential evaporation from a larger parent can not explain the multiplicities in the higher energy region. This is already suggested by the energy dependence of various multiplicities in Figure 8 as well as by much of the discussion in the previous section. Thus we do not employ this method based on slope measurements above 5.6 MeV/nucleon .

B. High Excitation (I) - the Vapor-Dominated Region

The double isotope ratio temperature technique proposed by Albergo *et al.* [71] has been extensively discussed and used in many experiments and theoretical calculations. Application of this technique assumes that thermal equilibration and chemical equilibration have been attained. In an experimental determination, one of the major problems is that secondary decay effects can modify the initial temperature strongly [74, 75, 76].

The experimental apparent double isotope temperature, T_{H-He} , can be deduced from the ratio of $\frac{M_d/M_t}{M_{^3He}/M_\alpha}$:

$$T_{H-He} = \frac{14.3}{\ln[1.59(M_d \cdot M_\alpha)/(M_t \cdot M_{^3He})]}, \quad (25)$$

where M_d , M_t , $M_{^3He}$, and M_α are the isotopic yields

of $d, t, ^3\text{He}$ and α from QP (see Fig. 8), respectively. As shown in Fig. 27 (solid squares), the apparent isotopic temperatures are well below those of the simple Fermi gas assumption (dotted line in the figure) indicating a strong influence due to secondary decay. To estimate the secondary decay effect Quantum Statistical Model (QSM) calculations were performed to correct the observed double isotope H-He ratio temperatures (T_{H-He}) for these effects.

For this purpose we compared results of two different calculations, the first published in reference [43, 76] and the second carried out for this work employing the QSM model described in reference [74, 75, 76]. The results of the two QSM models are in quite good agreement with each other. For nuclei with $A \sim 36$ in the excitation energy range of Interest, averaging results of these models indicates that $T_{init} = (1.75 \pm 0.06) \times T_{HHe}$. The corrected isotopic temperature is shown in Fig. 28 as the solid circles.

As emphasized above, this method is based on a model which assumes simultaneous fragmentation of a reduced density equilibrated nucleus and subsequent secondary evaporation from the primary fragments [74]. This method should be inappropriate in the lower excitation energy where the vapor assumption of the QSM is violated. In this case, we do not apply the technique below 5 MeV/nucleon

The two techniques differ somewhat in the excitation energy range near the transition point, indicating some systematic error due to using different techniques in the transition point region. This supports the argument for restricting the use of each technique to the "appropriate" excitation energy region.

We note that the caloric curve, defined in this manner, exhibits no obvious plateau. A polynomial fit to the data points leads to a temperature at the transition point of 8.3 ± 0.5 MeV.

C. High Excitation (II) - the Ideal Vapor Assumption

If the vapor phase may be characterized as an ideal gas of clusters [13], then, at and above $T = 8.3$ MeV, this should be signaled by a kinetic temperature, $T_{kin} = \frac{2}{3}E_{kin}^{th}$, where E_{kin}^{th} is the Coulomb corrected average kinetic energy of primary fragments. Secondary decay effects make it difficult to test this expectation. However, in an inspection of the average kinetic energies or apparent slope parameters (Fig. 27) for the different species observed , we find that, *for each excitation energy window*, the average kinetic energy of ^3He isotropically emitted in the projectile like frame, is higher than those of other species. This together with simple model estimates indicates that the ^3He spectra are the least affected by secondary decay. Kinetic temperatures for ^3He , defined as $\frac{2}{3}(\bar{E}_k - B_c)$ where \bar{E}_k is the average kinetic energy and B_c is the Coulomb energy(obtained from the fits), are

plotted as open squares in Fig. 28. Above $T = 8.3$ MeV the kinetic temperatures show a similar trend to that of the chemical temperatures but are approximately 1.5 MeV lower. While not perfect this approximate agreement provides additional evidence for disassembly of an equilibrated system.

For heavier systems a plateau or flattening is often observed in caloric curves [1] and the region of entry into the plateau appears to be very close to the point which has been identified as the point of maximal fluctuations. The reason for this flattening is still under discussion. It may reflect expansion and/or spinodal decomposition inside the coexistence region [18, 77, 78, 79, 80, 81]. In contrast, our light system does not show the flattening. This suggests which that the transition under investigation may differ from that seen in the heavier systems.

Taken together with the observations indicating maximal fluctuations and the particular features of the fragment topological structure at 5.6 MeV/u excitation, the comportment of this caloric curve provides further evidence suggesting that the observed transition is taking place at, or very close to, the critical point.

VII. DETERMINATION OF CRITICAL EXPONENTS

Since the pioneering work on extraction of the critical exponents for nuclear multifragmentation from EOS data [82], several additional experimental and theoretical efforts have been attempted [11, 83, 84, 85]. In the latter works, Elliott *et al.* show that the scaling behavior can remain even in small systems and the critical exponents can be extracted.

In the Fisher droplet model, the critical exponent τ can be deduced from the cluster distribution near the phase transition point. In Sec. V(A), we already determined, from the yield distributions, $\tau_{eff} \sim 2.31 \pm 0.03$, which is close to that for the liquid gas phase transition universality class. In terms of the scaling theory, τ can also be deduced from, (S_{corr}) , the slope of the correlation between $\ln(S_3)$ vs $\ln(S_2)$ [83], where $S_3 = M_3/M_1$, shown in Fig. 29, is related to τ as

$$\tau = \frac{3S_{corr} - 4}{S_{corr} - 1}. \quad (26)$$

Assuming the value of $T_c = 8.3$ MeV as determined from our caloric curve measurements, we explored the correlation of S_2 and S_3 in two ranges of excitation energy C see Figure 31. The moments were computed by exclusion of the species with Z_{max} in the "liquid" phase but inclusion in the "vapor" phase. The slopes were determined from linear fits to the "vapor" and "liquid" regions respectively and then averaged. In this way, we obtained a value of $\tau = 2.13 \pm 0.1$. See Fig. 29.

Other critical exponents can also be related to other moments of cluster distribution, M_k , which were defined in Eq. 14. Since, for our system, we have already deduced

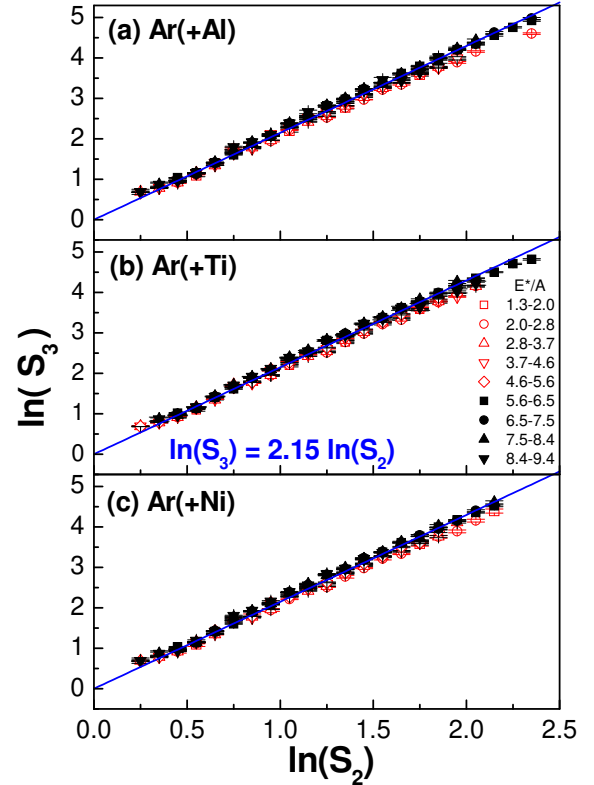


FIG. 29: (Color online) The correlation of between $\ln(S_3)$ vs $\ln(S_2)$ and the linear fit.

the initial temperatures and determined a critical temperature $T_c = 8.3$ MeV at point of maximal fluctuations, we can use temperature as a control parameter for such determinations. In this context, the critical exponent β can be extracted from the relation

$$Z_{max} \propto (1 - \frac{T}{T_c})^\beta, \quad (27)$$

and the critical exponent γ can be extracted from the second moment via

$$M_2 \propto |1 - \frac{T}{T_c}|^{-\gamma}. \quad (28)$$

In each, $|1 - \frac{T}{T_c}|$ is the parameter which measures the distance from the critical point.

Fig. 30 explores the dependence of Z_{max} on $(\frac{T}{T_c})$. We note a dramatic change of Z_{max} around the critical temperature T_c . LGM calculations also predict that the slope of Z_{max} vs T will change at the liquid gas phase transition [86]. Physically, the largest fragment is simply related to the order parameter $\rho_l - \rho_g$ (the difference of density in nuclear 'liquid' and 'gas' phases). In infinite matter, the infinite cluster exists only on the 'liquid' side of the critical point. In finite matter, the largest cluster is present on both sides of the phase transition point. In this figure, the significant change of the slope of Z_{max} with temperature should correspond to a sudden disappearance of

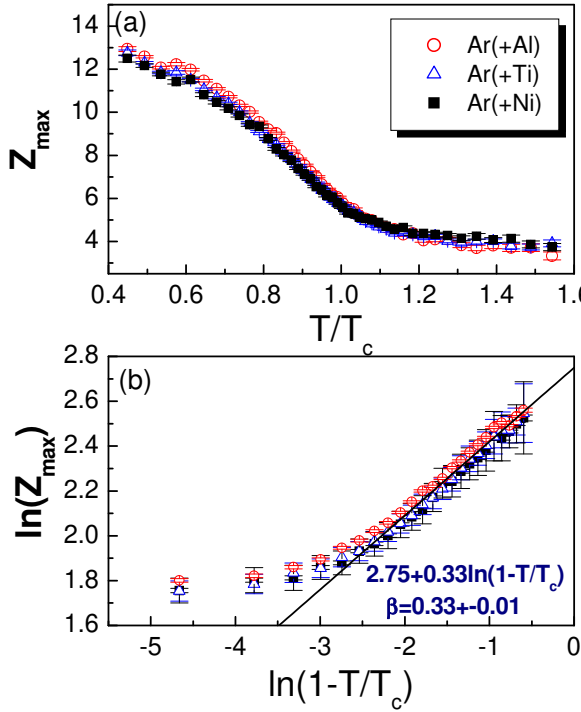


FIG. 30: (Color online) Z_{\max} as a function of T/T_c (a) and the extraction of the critical exponent β (b).

the infinite cluster ('bulk liquid') near the phase transition temperature. For the finite system, it reflects the onset of critical behavior there. Using the left side of this curve (*i.e.* liquid side), we can deduce the critical exponent β by the transformation of the x axis variable to the distance from the critical point. Fig. 30b shows the extraction of β using Eq. 27. An excellent fit was obtained in the region away from the critical point, which indicates a critical exponent $\beta = 0.33 \pm 0.01$. Near the critical point, the finite size effects become stronger so that the scaling law is violated. The extracted value of β is that expected for a liquid gas transition (See Table.II) [53].

To extract the critical exponent γ , we take M_2 on the liquid side without Z_{\max} but take M_2 on the vapor side with Z_{\max} included. Fig. 31 shows $\ln(M_2)$ as a function of $\ln(|1 - \frac{T}{T_c}|)$. The lower set of points is from the liquid phase and the upper set of points is from the vapor phase. For the liquid component, we center our fit to Eq. 28 about the center of the range of $(1 - T/T_c)$ which leads to the linear fit and extraction of β as represented in Figure. 30. We obtain the critical exponent $\gamma = 1.15 \pm 0.06$. This value of γ is also close to the value expected for the liquid gas universality class (see Table II). It is seen that the selected region has a good power law dependence. However, a similar effort to extract the γ in

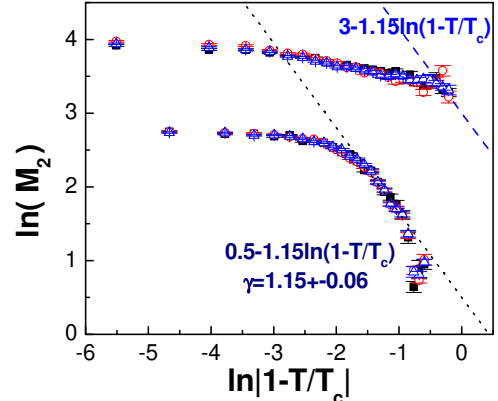


FIG. 31: (Color online) The extraction of critical exponents γ . See texts for details.

the gas phase is not successful: a small value less than 0.20 is deduced. This may be due to the finite size effects for this very light system. Since the largest cluster still exists in the vapor side, its inclusion (or exclusion) in M_2 might perturb the determination of the moment, resulting in an imprecise value of γ extracted from the vapor phase. For comparison, we just show, for the vapor phase, a line representing the γ derived from the liquid side. This line only agrees with the last few vapor points, *i.e.* the highest temperature points (the contamination of M_2 should be the least there).

Since we have the critical exponent β and γ , we can use the scaling relation

$$\sigma = \frac{1}{\beta + \gamma}, \quad (29)$$

to derive the critical exponent σ . In such way, we get the $\sigma = 0.68 \pm 0.04$, which is also very close to the expected critical exponent of a liquid gas system.

Finally, it is possible to use the scaling relation

$$\tau = 2 + \frac{\beta}{\beta + \gamma}, \quad (30)$$

to check the τ value which was determined from the charge distributions using Fisher droplet model power law fits around the critical point (see Fig. 9). Using Eq. 30 we Obtain $\tau = 2.22 \pm 0.46$, which, though less precise, is in agreement with the values of 2.31 ± 0.03 obtained from the charge distribution around the point of maximal fluctuations and 2.15 ± 0.1 extracted from the correlation of $\ln(S_3)$ vs $\ln(S_2)$.

To summarize this section, we report in Table.II a comparison of our results with the Values expected for the 3D percolation and liquid gas system universality classes and with the results obtained by Elliott et al. for a heavier system. Obviously, our values for this light system with $A \sim 36$ are consistent with the values of the liquid gas phase transition universality class rather the 3D percolation class.

TABLE II: Comparison of the Critical Exponents

Exponents 3D Percolation		Liquid-Gas	This work
			2.22±0.46 (Eq. 30)
τ	2.18	2.21	2.31±0.03 (Eq. 12)
			2.13±0.10 (Eq. 26)
β	0.41	0.33	0.33±0.01
γ	1.8	1.23	1.15±0.06
σ	0.45	0.64	0.68±0.04

VIII. CONCLUSIONS

In conclusion, an extensive survey of the features of the disassembly of nuclei with $A \sim 36$ has been reported. To carry out this analysis, the de-excitation products of the $A \sim 36$ quasi projectile source were first reconstructed using a new technique based upon the three source fits to the light particle spectra and use of a rapidity cut for IMF. Monte Carlo sampling techniques were applied to assign all particles to one of three sources (QP, NN and QT).

At an excitation energy ~ 5.6 MeV/nucleon key observables demonstrate the existence of maximal fluctuations in the disassembly process. These fluctuation observables include the Campi scattering plots and the normalized variances of the distributions of order parameters, (Z_{max}) and total kinetic energy. Recently proposed Δ -scaling analysis also show a universal behavior at higher excitation energy where the saturation of the reduced fluctuations of Z_{max} (*i.e.* $\frac{\sigma Z_{max}}{\langle Z_{max} \rangle}$) is observed. This corresponds to the transition to a regime of large fluctuations from an ordered phase at lower excitation energy.

At the same excitation energy ~ 5.6 MeV/nucleon, the Fisher droplet model prediction is satisfied, with a Fisher power law parameter, $\tau = 2.3$, close to the critical exponent of the liquid gas phase transition universality class. In addition, the fragment topological structure shows that the rank sorted fragments obey Zipf's law, proposed as a signature of liquid gas phase transition [63], at the maximal fluctuation point. The related phase separation parameter [68] shows a significant change of slope

with excitation energy. The correlation of the heaviest fragment and the second heaviest fragment demonstrates a transition around 5.6 MeV/u of excitation energy. A bimodality test [69] also gives an indication of a phase change in the same excitation energy region.

The caloric curve shows a monotonic increase in temperature and no plateau region is apparent, in contrast to caloric curves seen for heavier systems [1]. At the apparent critical excitation energy the temperature is 8.3 ± 0.5 MeV. Taking this to be the critical temperature for this system, we extracted the critical exponents β , γ and σ . The deduced values are consistent with the values of the liquid gas phase transition universality class [53].

Since some fluctuation observables, such as the structure of the Campi plot, Z_{max} fluctuations etc., could be produced by mass conservation effects where no assumption of the critical behavior is needed, these observables by themselves do not guarantee that the critical point has been reached. What differentiates the present work from previous identifications of points of critical behavior in nuclei, in addition to the fact that these are the lightest nuclei for which a detailed experimental analysis has been made, is the comportment of the caloric curve and the critical exponent extraction. Taken together, this body of evidence suggests a liquid gas phase change in an equilibrated system at, or extremely close to, the critical point. Detailed theoretical confrontations with models which include or exclude a liquid gas phase transition are certainly interesting and welcome. Some work along this line is in progress [87, 88].

Acknowledgments

This work was supported by the U.S. Department of Energy and the Robert A. Welch Foundation under Grant No. A330. The work of YGM is also partially supported by the NSFC under Grant No. 19725521 and the Major State Basic Research Development Program in China under Contract No. G2000077404. YGM is also grateful to Texas A&M University - Cyclotron Institute for support and hospitality extended to him. R.A., A.M-D and A. M-R wish to acknowledge partial support from DGAPA and CONACYT-Mexico.

[1] J. B. Natowitz, R. Wada, K. Hagel, T. Keutgen, M. Murray, A. Makeev, L. Qin, P. Smith, and C. Hamilton , Phys. Rev. C **65**, 034618 (2002).

[2] J. B. Natowitz, K. Hagel, Y. G. Ma, M. Murray, L. Qin, R. Wada, and J. Wang, Phys. Rev. Lett. **89**, 212701 (2002).

[3] X. Campi, J. Phys. A **19**, L917 (1986);
X. Campi, Phys. Lett. B **208**, 351 (1988).

[4] J. Richert and P. Wagner, Phys. Rep. **350**, 1 (2001).

[5] S. Das Gupta, A. Z. Mekjian, M. B. Tsang, Adv. Nucl. Phys. **26** , 89 (2001).

[6] A. Bonasera, M. Bruno, C. O. Dorso, P. F. Mastinu, Riv. Del Nuovo. Cim. **23**, 1 (2000).

[7] Ph. Chomaz, Proceedings of the INPC 2001 Conference, Berkeley, Ca., July 2001.

[8] L.G. Moretto, J. B. Elliott, L. Phair, G. J. Wozniak, C. M. Mader, and A. Chappars, Proceedings of the INPC 2001 Conference, Berkeley, Ca., July 2001.

[9] J. C. Pan, S. Das Gupta and M. Grant, Phys. Rev. Lett. **80**, 1182 (1998).

[10] F. Gulminelli and Ph. Chomaz, Phys. Rev. Lett. **82**, 1402 (1999);

Ph. Chomaz, V. Duflot, and F. Gulminelli, Phys. Rev. Lett. **85**, 3587 (2000).

[11] J. B. Elliott, S. Albergo, F. Bieser, F. P. Brady, Z. Caccia, D. A. Cebra, A. D. Chacon, J. L. Chance, Y. Choi, S. Costa, M. L. Gilkes, J. A. Hauger, A. S. Hirsch, E. L. Hjort, A. Insolia, M. Justice, D. Keane, J. C. Kintner, V. Lindenstruth, M. A. Lisa, H. S. Matis, M. McMahan, C. McParland, W. F. J. Müller, D. L. Olson, M. D. Partlan, N. T. Porile, R. Potenza, G. Rai, J. Rasmussen, H. G. Ritter, J. Romanski, J. L. Romero, G. V. Russo, H. Sann, R. P. Scharenberg, A. Scott, Y. Shao, B. K. Srivastava, T. J. M. Symons, M. Tincknell, C. Tuvé, S. Wang, P. G. Warren, H. H. Wieman, T. Wienold, and K. Wolf, Phys. Rev. C **62**, 064603 (2000).

[12] J. B. Elliott, L. G. Moretto, L. Phair, G. J. Wozniak, L. Beaulieu, H. Breuer, R. G. Korteling, K. Kwiatkowski, T. Lefort, L. Pienkowski, A. Ruangma, V. E. Viola, and S. J. Yennello, Phys. Rev. Lett. **88**, 042701 (2002).

[13] M. E. Fisher, Rep. Prog. Phys. **30**, 615 (1969); Physics **3**, 255 (1967).

[14] J. A. Hauger, P. Warren, S. Albergo, F. Bieser, F. P. Brady, Z. Caccia, D. A. Cebra, A. D. Chacon, J. L. Chance, Y. Choi, S. Costa, J. B. Elliott, M. L. Gilkes, A. S. Hirsch, E. L. Hjort, A. Insolia, M. Justice, D. Keane, J. C. Kintner, V. Lindenstruth, M. A. Lisa, H. S. Matis, M. McMahan, C. McParland, W. F. J. Müller, D. L. Olson, M. D. Partlan, N. T. Porile, R. Potenza, G. Rai, J. Rasmussen, H. G. Ritter, J. Romanski, J. L. Romero, G. V. Russo, H. Sann, R. P. Scharenberg, A. Scott, Y. Shao, B. K. Srivastava, T. J. M. Symons, M. Tincknell, C. Tuvé, S. Wang, H. H. Wieman, T. Wienold, and K. Wolf, Phys. Rev. C **57**, 764 (1998); J. A. Hauger, B. K. Srivastava, S. Albergo, F. Bieser, F. P. Brady, Z. Caccia, D. A. Cebra, A. D. Chacon, J. L. Chance, Y. Choi, S. Costa, J. B. Elliott, M. L. Gilkes, A. S. Hirsch, E. L. Hjort, A. Insolia, M. Justice, D. Keane, J. C. Kintner, V. Lindenstruth, M. A. Lisa, H. S. Matis, M. McMahan, C. McParland, W. F. J. Müller, D. L. Olson, M. D. Partlan, N. T. Porile, R. Potenza, G. Rai, J. Rasmussen, H. G. Ritter, J. Romanski, J. L. Romero, G. V. Russo, H. Sann, R. P. Scharenberg, A. Scott, Y. Shao, T. J. M. Symons, M. Tincknell, C. Tuvé, S. Wang, P. Warren, H. H. Wieman, T. Wienold, and K. Wolf, Phys. Rev. C **62**, 024616 (2000).

[15] L. Beaulieu, T. Lefort, K. Kwiatkowski, R. T. de Souza, W.-c. Hsi, L. Pienkowski, B. Back, D. S. Bracken, H. Breuer, E. Cornell, F. Gimeno-Nogues, D. S. Ginger, S. Gushue, R. G. Korteling, R. Laforest, E. Martin, K. B. Morley, E. Ramakrishnan, L. P. Remsberg, D. Rowland, A. Ruangma, V. E. Viola, G. Wang, E. Winchester, and S. J. Yennello, Phys. Rev. Lett. **84**, 5971 (2000).

[16] M. Kleine Berkenbusch, W. Bauer, K. Dillman, S. Pratt, L. Beaulieu, K. Kwiatkowski, T. Lefort, W.-c. Hsi, and V. E. Viola, S. J. Yennello, R. G. Korteling, and H. Breuer, Phys. Rev. Lett. **88**, 022701 (2002).

[17] J. B. Elliott, L. G. Moretto, L. Phair, G. J. Wozniak, S. Albergo, F. Bieser, F. P. Brady, Z. Caccia, D. A. Cebra, A. D. Chacon, J. L. Chance, Y. Choi, S. Costa, M. L. Gilkes, J. A. Hauger, A. S. Hirsch, E. L. Hjort, A. Insolia, M. Justice, D. Keane, J. C. Kintner, V. Lindenstruth, M. A. Lisa, H. S. Matis, M. McMahan, C. McParland, W. F. J. Müller, D. L. Olson, M. D. Partlan, N. T. Porile, R. Potenza, G. Rai, J. Rasmussen, H. G. Ritter, J. Romanski, J. L. Romero, G. V. Russo, H. Sann, R. P. Scharenberg, A. Scott, Y. Shao, B. K. Srivastava, T. J. M. Symons, M. Tincknell, C. Tuvé, S. Wang, P. Warren, H. H. Wieman, T. Wienold, and K. Wolf, Phys. Rev. C **65**, 053201 (R) (2002).

[32] Al. H. Raduta and Ad. R. Raduta, Phys. Rev. Lett. **87**, 202701 (2001).

[33] <http://cyclotron.tamu.edu/NIMROD>

[34] J. Péter, S. C. Jeong, J. C. Angélique, G. Auger, G. Bizard, R. Brou, A. Buta, C. Cabot, Y. Cassagnou, E. Crema, D. Cussol, D. Durand, Y. El Masri, P. Eudes, Z. Y. He, A. Kerambrun, C. Lebrun, R. Legrain, J. P. Patry, A. Péghaire, R. Régimbart, E. Rosato, F. Saint-Laurent, J. C. Steckmeyer, B. Tamain and E. Vient, Nucl. Phys. A **593**, 95 (1995).

[35] J. C. Steckmeyer, A. Kerambrun, J. C. Angélique, G. Auger, G. Bizard, R. Brou, C. Cabot, E. Crema, D. Cussol, D. Durand, Y. El Masri, P. Eudes, M. Gonin, K.

Hagel, Z. Y. He, S. C. Jeong, C. Lebrun, J. P. Patry, A. Péghaire, J. Péter, R. Régimbart, E. Rosato, F. Saint-Laurent, B. Tamain, E. Vient, and R. Wada, Phys. Rev. Lett. **76**, 4895 (1996).

[36] G. Tabcaru, B. Borderie, A. Ouatizerga, M. Pârlig, M. F. Rivet, G. Auger, Ch. O. Bacri, F. Bocage, R. Bougault, R. Brou, Ph. Buche, J. L. Charvet, A. Chbihi, J. Colin, D. Cussol, R. Dayras, A. Demeyer, D. Doré, D. Durand, P. Ecomard, J. D. Frankland, E. Galichet, E. Genouin-Duhamel, E. Gerlic, D. Guinet, P. Lautesse, J. L. Laville, A. Le Févre, T. Lefort, R. Legrain, N. Le Neindre, O. Lopez, M. Louvel, L. Nalpas, A. D. Nguyen, E. Plagnol, E. Rosato, F. Saint-Laurent, S. Salou, M. Squalli, J. C. Steckmeyer, M. Stern, L. Tassan-Got, O. Tirel, E. Vient, C. Volant and J. P. Wieleczko, Nucl. Inst. Method A **428**, 379 (1999).

[37] F. Benrachi, B. Chambon, B. Cheynis, D. Drain, C. Pastor, D. Seghier and K. Zaid, A. Giorni, D. Heuer, A. Llères, C. Morand, P. Stassi and J. B. Viano, Nucl. Inst. Method A **281**, 137 (1989).

[38] R. Planeta, W. Gawlikowicz, A. Wieloch, J. Brzychczyk, T. Ciszek, A.J. Cole, P. Desquelles, K. Grotowski, P. Hachaj, S. Micek, P. Pawlowski, Z. Sosin, D. Benchekroun, E. Bisquer, A. Chabane, M. Charvet, B. Cheynis, A. Demeyer, E. Gerlic, A. Giorni, D. Guinet, D. Heuer, P. Lautesse, L. Lebreton, A. Llères, M. Stern, L. Vagneron and J.B. Viano, Eur. Phys. J. A **11**, 297 (2001).

[39] Z. Sosin, R. Planeta, T. Ciszek, J. Brzychczyk, W. Gawlikowicz, K. Grotowski, S. Micek, P. Pawlowski, A. Wieloch, A.J. Cole, D. Benchekroun, E. Bisquer, A. Chabane, M. Charvet, B. Cheynis, A. Demeyer, E. P. Desquelles, E. Gerlic, A. Giorni, D. Guinet, D. Heuer, P. Lautesse, L. Lebreton, A. Llères, M. Stern, L. Vagneron and J.B. Viano, Eur. Phys. J. A **11**, 305 (2001).

[40] Y. G. Ma, A. Siwek, J. Péter, F. Gulminelli, R. Dayras, L. Nalpas, B. Tamain, E. Vient, G. Auger, Ch.O. Bacri, J. Benlliure, E. Bisquer, B. Borderie, R. Bougault, R. Brou, J. L. Charvet, A. Chibi, J. Colin, D. Cussol, E. De Filippo, A. Demeyer, D. Dore, D. Durand, E. Ecomard, Ph. Eudes, E. Gerlic, D. Gourio, D. Guinet, R. Laforest, P. Lautesse, J. L. Laville, L. Lebreton, J. F. Lecolley, A. Le Fevre, T. Lefort, R. Legrain, O. Lopez, M. Louvel, J. Lukasik, N. Marie, V. Metivier, A. Ouatizerga, M. Parlog, E. Plagnol, A. Rahman, T. Reposeur, M.F. Rivet, E. Rosato, F. Saint-Laurent, M. Squalli, J.C. Steckmeyer, M. Stern, L. Tassan-got, C. Volant, and J. P. Wieleczko, Phys. Lett. B **390**, 41 (1997).

[41] T. C. Awes, G. Poggi, C. K. Gelbke, B. B. Black, B. G. Glagola, H. Breuer, and V. E. Viola, Phys. Rev. C **24**, 89 (1981).

[42] D. Prindle, A. Elmaani, C. Hyde-Wright, W. Jiang, A. A. Sonzogni, R. Vandebosch, D. Bowman, G. Cron, P. Danielewicz, J. Dinius, W. Hsi, W. G. Lynch, C. Montoya, G. Peaslee, C. Schwarz, M. B. Tsang, C. Williams, R. T. de Souza, D. Fox, and T. Moore, Phys. Rev. C **57**, 1305 (1998).

[43] D. Cussol, G. Bizard, R. Brou, D. Durand, M. Louvel, J. P. Patry, J. Péter, R. Regimbart, J. C. Steckmeyer, J. P. Sullivan, B. Tamain, E. Crema, b, H. Doubre, K. Hagel, G. M. Jin, A. Péghaire, F. Saint-Laurent, Y. Cassagnou, R. Legrain, C. Lebrun, E. Rosato, R. MacGrath, S. C. Jeong, S. M. Lee, Y. Nagashima, T. Nakagawa, M. Ogihara, J. Kasagi, and T. Motobayashi, Nucl. Phys. A **561**, 298 (1993).

[44] K. Sümmerer, W. Brüchle, D. J. Morrissey, M. Schädel, B. Szweryn, and Yang Weifan, Phys. Rev. C **42**, 2546 (1990).

[45] Y. G. Ma *et al.*, unpublished.

[46] C. A. Ogilvie, J. C. Adloff, M. Begemann-Blaich, P. Bouissou, J. Hubele, G. Imme, I. Iori, P. Kreutz, G. J. Kunde, S. Leray, V. Lindenstruth, Z. Liu, U. Lynen, R. J. Meijer, U. Milkau, W. F. J. Müller, C. Ng, J. Pochodzalla, G. Raciti, G. Rudolf, H. Sann, A. Schüttauf, W. Seidel, L. Stuttge, W. Trautmann, and A. Tucholski, Phys. Rev. Lett. **67**, 1214 (1991).

[47] M. B. Tsang, W. C. Hsi, W. G. Lynch, D. R. Bowman, C. K. Gelbke, M. A. Lisa, G. F. Peaslee, G. J. Kunde, M. L. Begemann-Blaich, T. Hofmann, J. Hubele, J. Kempter, P. Kreutz, W. D. Kunze, V. Lindenstruth, U. Lynen, M. Mang, W. F. J. Müller, M. Neumann, B. Ocker, C. A. Ogilvie, J. Pochodzalla, F. Rosenberger, H. Sann, A. Schüttauf, V. Serfling, J. Stroth, W. Trautmann, A. Tucholski, A. Wörner, E. Zude, B. Zwieglinski, S. Aiello, G. Immé, V. Pappalardo, G. Raciti, R. J. Charity, L. G. Sobotka, I. Iori, A. Moroni, R. Scardoni, A. Ferrero, W. Seidel, Th. Blaich, L. Stuttge, A. Cosmo, W. A. Friedman, G. Peilert, Phys. Rev. Lett. **71**, 1502 (1993).

[48] Y. G. Ma and W. Q. Shen, Phys. Rev. C **51**, 710 (1995).

[49] M. E. Finn, S. Agarwal, A. Bujak, J. Chuang, L. J. Gutay, A. S. Hirsch, R. W. Minich, N. T. Porile, R. P. Scharenberg, B. C. Stringfellow, and F. Turkot, Phys. Rev. Lett. **49**, 1321 (1982).

[50] A. S. Hirsch, A. Bujak, J. E. Finn, L. J. Gutay, R. W. Minich, N. T. Porile, R. P. Scharenberg, B. C. Stringfellow, and F. Turkot, Phys. Rev. C **29**, 508 (1984).

[51] R. W. Minich, S. Agarwal, A. Bujak, J. Chuang, J. E. Finn, L. J. Gutay, A. S. Hirsch, N. T. Porile, R. P. Scharenberg and B. C. Stringfellow, Phys. Lett. **118B**, 458 (1982).

[52] F. Gulminelli and Ph. Chomaz, Int. J. Mod. Phys. E **8**, 527 (1999).

[53] H. E. Stanley, Introduction to Phase Transitions and Critical Phenomena, Oxford University Press, Cambridge, England, 1992.

[54] X. Campi and H. Krivine, Nucl. Phys. A **545**, 161 c (1992).

[55] X. Campi and H. Krivine, Z. Phys. A **344**, 81 (1992).

[56] B. Elattari, J. Richert and P. Wagner, Phys. Rev. Lett. **69**, 45 (1992);
B. Elattari, J. Richert and P. Wagner, Nucl. Phys. A **560**, 603 (1993).

[57] Ph. Chomaz and F. Gulminelli, Nucl. Phys. A **647**, 153 (1999);
J. L. Lebowitz, J. K. Percus, and L. Verlet, Phys. Rev. **153**, 250 (1967).

[58] Ph. Chomaz, V. Duflot and F. Gulminelli, Phys. Rev. Lett. **85**, 3587 (2000).

[59] M. D'Agostino, F. Gulminelli, Ph. Chomaz, M. Bruno, F. Cannata, R. Bougault, F. Gramegna, I. Iori, N. Le Neindre, G. V. Margagliotti, A. Moroni and G. Vannini Phys. Lett. B **473**, 219 (2000).

[60] K. S. Huang, Statistical Mechanics, J. Wiley and Sons 1963, chapt. 6.

[61] R. Botet and M. Ploszajczak, Phys. Rev. E **62**, 1825 (2000).

[62] J.D. Frankland, A. Chbihi, A. Mignon, M.L. Begemann-Blaich, R. Bittiger, B. Borderie, R. Bougault, J.-L.

Charvet, D. Cussol, R. Dayras, D. Durand, C. Escano-Rodriguez, E. Galichet, D. Guinet, P. Lautesse, A. Le Fevre, R. Legrain, N. Le Neindre, O. Lopez, J. Lukasik, U. Lynen, L. Manduci, J. Marie, W.F.J. Muller, H. Orth, M. Parlog, M. Pichon, M. F. Rivet, E. Rosato, R. Roy, A. Saija, C. Schwarz, C. Sfienti, B. Tamain, W. Trautmann, A. Traczinski, K. Turzo, A. Van Lauwe, M. Vigilante, C. Volant, J.P. Wieleczko, B. Zwieginski, ArXiv nucl-ex/0404024

[63] Y. G. Ma, Phys. Rev. Lett. **83**, 3617 (1999).

[64] Y. G. Ma, Eur. Phys. J. A **6**, 367 (1999).

[65] G. K. Zipf, *Human Behavior and the Principle of Least Effort* (Addison-Wesley, Cambridge, MA, 1949); D. Crystal, *The Cambridge Encyclopedia of Language* (Cambridge University, Cambridge, England, 1987), p. 86.

[66] D. L. Turcotte, Rep. Prog. Phys. **62**, 1377 (1999).

[67] A. Dabrowska, M. Szarska, A. Trzupek, W. Wolter, B. Bosiek, Acta Phys. Pol. B **35**, 2109(2004); Acta Phys. Pol. B **32**, 3099 (2001).

[68] A. J. Cole, Phys. Rev. C **65**, 031601R (2002).

[69] Ph. Chomaz, F. Gulminelli and V. Duflot, Phys. Rev. E **64**, 046114 (2001).

[70] B. Borderie, J. Phys. G **28**, R217 (2002).

[71] S. Albergo, S. Costa, E. Costanzo, A. Rubbino, Nuovo Cimento A **89A**, 1 (1985).

[72] K. Hagel, D. Fabris, P. Gonthier, H. Ho, Y. Lou, Z. Majka, G. Mouchaty, M. N. Namboodiri, J. B. Natowitz, G. Nebbia, R. P. Schmitt, G. Viesti, R. Wada and B. Wilkins, Nucl. Phys. A **486**, 429 (1988).

[73] R. Wada, D. Fabris, K. Hagel, G. Nebbia, Y. Lou, M. Gonin, J. B. Natowitz, R. Billerey, B. Cheynis, A. Demeyer, D. Guinet, C. Pastor, L. Vagneron, K. Zaid, J. Alarja, A. Giorni, D. Heuer, C. Morand, B. Viano, C. Mazur, C. Ngô, S. Leray, R. Lucas, M. Ribrag, and E. Tomasi, Phys. Rev. C **39**, 497 (1989).

[74] D. Hahn and H. Stöcker, Nucl. Phys. A **476**, 718 (1988); J. Konopka, H. Graf, H. Stöcker, and W. Greiner, Phys. Rev. C **50**, 2085 (1994).

[75] Z. Majka, P. Staszek, J. Cibor, J. B. Natowitz, K. Hagel, J. Li, N. Mdeiwayeh, R. Wada, and Y. Zhao, Phys. Rev. C **55**, 2991 (1997).

[76] F. Gulminelli and D. Durand, Nucl. Phys. A **615**, 117 (1997).

[77] A. Strachan and C. O. Dorso, Phys. Rev. C **58**, R632 (1998).

[78] J. B. Natowitz, K. Hagel, Y. G. Ma, M. Murray, L. Qin, S. Sholomo, R. Wada, and J. Wang, Phys. Rev. C **66**, 031601 (2002).

[79] T. Furuta and A. Ono, ArXiv:nucl-th/0305050.

[80] V. E. Viola, K. Kwiatkowski, J. B. Natowitz, and S. J. Yennello, Phys. Rev. Lett. **93**, 132701 (2004).

[81] L. G. Sobotka, R. J. Charity, J. Töke, and W. U. Schröder, Phys. Rev. Lett. **93**, 132702 (2004).

[82] M. L. Gilkes, S. Albergo, F. Bieser, F. P. Brady, Z. Caccia, D. A. Cebra, A. D. Chacon, J. L. Chance, Y. Choi, S. Costa, J. B. Elliott, J. A. Hauger, A. S. Hirsch, E. L. Hjort, A. Insolia, M. Justice, D. Keane, J. C. Kintner, V. Lindenstruth, M. A. Lisa, U. Lynen, H. S. Matis, M. McMahan, C. McParland, W. F. J. Müller, D. L. Olson, M. D. Partlan, N. T. Porile, R. Potenza, G. Rai, J. Rasmussen, H. G. Ritter, J. Romanski, J. L. Romero, G. V. Russo, H. Sann, R. Scharenberg, A. Scott, Y. Shao, B. K. Srivastava, T. J. M. Symons, M. Tincknell, C. Tuvé, S. Wang, P. Warren, H. H. Weiman, and K. Wolf, Phys. Rev. Lett. **73**, 1590 (1994).

[83] M. D'Agostino, A. S. Botvina, M. Bruno, A. Bonasera, J. P. Bondorf, R. Bougault, P. Désesquelles, f, E. Geraci, F. Gulminelli, I. Iori, N. Le Neindre, G. V. Margagliotti, I. N. Mishustin, A. Moroni, A. Pagano and G. Vannin, Nucl. Phys. A **650**, 329 (1999).

[84] J. B. Elliott, M. L. Gilkes, J. A. Hauger, A. S. Hirsch, E. Hjort, N. T. Porile, R. P. Scharenberg, B. K. Srivastava, M. L. Tincknell, and P. G. Warren, Phys. Rev. C **55**, 1319 (1997).

[85] J. B. Elliott, M. L. Gilkes, J. A. Hauger, A. S. Hirsch, E. Hjort, N. T. Porile, R. P. Scharenberg, B. K. Srivastava, M. L. Tincknell, and P. G. Warren, Phys. Rev. C **49**, 3185 (1994).

[86] Y. G. Ma, J. Phys. G **27**, 2455 (2001).

[87] Y. G. Ma *et al.*, in preparation.

[88] A. S. Botvina, SMM calculations and Private Communication.